

University of Groningen

Gitelman-Like Syndrome Caused by Pathogenic Variants in mtDNA

Genomics England Res Consortium; Viering, Daan; Schlingmann, Karl P.; Hureauux, Marguerite; Nijenhuis, Tom; Mallett, Andrew; Chan, Melanie M. Y.; van Beek, Andre; van Eerde, Albertien M.; Coulibaly, Jean-Marie

Published in:
Journal of the American Society of Nephrology

DOI:
[10.1681/ASN.2021050596](https://doi.org/10.1681/ASN.2021050596)

IMPORTANT NOTE: You are advised to consult the publisher's version (publisher's PDF) if you wish to cite from it. Please check the document version below.

Document Version
Publisher's PDF, also known as Version of record

Publication date:
2022

[Link to publication in University of Groningen/UMCG research database](#)

Citation for published version (APA):

Genomics England Res Consortium, Viering, D., Schlingmann, K. P., Hureauux, M., Nijenhuis, T., Mallett, A., Chan, M. M. Y., van Beek, A., van Eerde, A. M., Coulibaly, J.-M., Vallet, M., Decramer, S., Pelletier, S., Klaus, G., Komhoff, M., Beetz, R., Patel, C., Shenoy, M., Steenbergen, E. J., ... de Baaij, J. H. F. (2022). Gitelman-Like Syndrome Caused by Pathogenic Variants in mtDNA. *Journal of the American Society of Nephrology*, 33(2), 305-325. <https://doi.org/10.1681/ASN.2021050596>

Copyright

Other than for strictly personal use, it is not permitted to download or to forward/distribute the text or part of it without the consent of the author(s) and/or copyright holder(s), unless the work is under an open content license (like Creative Commons).



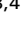




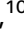








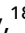



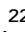
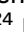
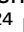

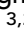





The publication may also be distributed here under the terms of Article 25fa of the Dutch Copyright Act, indicated by the "Taverne" license. More information can be found on the University of Groningen website: <https://www.rug.nl/library/open-access/self-archiving-pure/taverne-amendment>.

Take-down policy

If you believe that this document breaches copyright please contact us providing details, and we will remove access to the work immediately and investigate your claim.

Downloaded from the University of Groningen/UMCG research database (Pure): <http://www.rug.nl/research/portal>. For technical reasons the number of authors shown on this cover page is limited to 10 maximum.

Gitelman-Like Syndrome Caused by Pathogenic Variants in mtDNA

Daan Viering ¹, Karl P. Schlingmann ², Marguerite Hureau ^{3,4}, Tom Nijenhuis ⁵, Andrew Mallett ^{6,7}, Melanie M.Y. Chan ⁸, André van Beek ⁹, Albertien M. van Eerde ¹⁰, Jean-Marie Coulibaly ¹¹, Marion Vallet ¹², Stéphane Decramer ¹³, Solenne Pelletier ¹⁴, Günter Klaus ¹⁵, Martin Kömhoff ¹⁶, Rolf Beetz ¹⁷, Chirag Patel ⁷, Mohan Shenoy ¹⁸, Eric J. Steenbergen ¹⁹, Glenn Anderson ²⁰, Ernie M.H.F. Bongers ²¹, Carsten Bergmann ^{22,23}, Daan Panneman ²⁴, Richard J. Rodenburg ²⁴, Robert Kleta ^{8,25}, Pascal Houillier ^{3,26,27}, Martin Konrad ², Rosa Vargas-Poussou ^{3,4,26}, Nine V.A.M. Knoers ²⁸, Detlef Bockenhauer ^{8,29}, Jeroen H.F. de Baaij ¹ and the Genomics England Research Consortium*

Due to the number of contributing authors, the affiliations are listed at the end of this article.

ABSTRACT

Background Gitelman syndrome is the most frequent hereditary salt-losing tubulopathy characterized by hypokalemic alkalosis and hypomagnesemia. Gitelman syndrome is caused by biallelic pathogenic variants in *SLC12A3*, encoding the Na⁺-Cl⁻ cotransporter (NCC) expressed in the distal convoluted tubule. Pathogenic variants of *CLCNKB*, *HNF1B*, *FXSD2*, or *KCNJ10* may result in the same renal phenotype of Gitelman syndrome, as they can lead to reduced NCC activity. For approximately 10 percent of patients with a Gitelman syndrome phenotype, the genotype is unknown.

Methods We identified mitochondrial DNA (mtDNA) variants in three families with Gitelman-like electrolyte abnormalities, then investigated 156 families for variants in *MT-TI* and *MT-TF*, which encode the transfer RNAs for phenylalanine and isoleucine. Mitochondrial respiratory chain function was assessed in patient fibroblasts. Mitochondrial dysfunction was induced in NCC-expressing HEK293 cells to assess the effect on thiazide-sensitive ²²Na⁺ transport.

Results Genetic investigations revealed four mtDNA variants in 13 families: m.591C>T (*n*=7), m.616T>C (*n*=1), m.643A>G (*n*=1) (all in *MT-TF*), and m.4291T>C (*n*=4, in *MT-TI*). Variants were near homoplasmic in affected individuals. All variants were classified as pathogenic, except for m.643A>G, which was classified as a variant of uncertain significance. Importantly, affected members of six families with an *MT-TF* variant additionally suffered from progressive chronic kidney disease. Dysfunction of oxidative phosphorylation complex IV and reduced maximal mitochondrial respiratory capacity were found in patient fibroblasts. *In vitro* pharmacological inhibition of complex IV, mimicking the effect of the mtDNA variants, inhibited NCC phosphorylation and NCC-mediated sodium uptake.

Conclusion Pathogenic mtDNA variants in *MT-TF* and *MT-TI* can cause a Gitelman-like syndrome. Genetic investigation of mtDNA should be considered in patients with unexplained Gitelman syndrome-like tubulopathies.

JASN 33: 305–325, 2022. doi: <https://doi.org/10.1681/ASN.2021050596>

Gitelman syndrome (GS) is a recessively inherited renal tubulopathy caused by pathogenic variants in *SLC12A3*, which encodes the thiazide-sensitive Na⁺-Cl⁻ cotransporter (NCC). NCC mediates

reabsorption of sodium and chloride in the distal convoluted tubule (DCT).¹ GS is characterized by distal tubular salt wasting with secondary hyperaldosteronism, hypochloremic metabolic alkalosis,

hypokalemia, hypomagnesemia, and hypocalciuria. Common clinical manifestations of GS include muscle cramps, paresthesias, nocturia, salt craving, muscle weakness, and fatigue.²

GS may be phenocopied by a number of genetic and nongenetic conditions. Nongenetic causes include diuretic abuse, chronic laxative abuse, and chronic vomiting. The most important genetic differential diagnosis to pathogenic variants in *SLC12A3* is the presence of biallelic pathogenic variants in *CLCNKB*, which encodes the distal tubular basolateral chloride channel ClC-Kb. Such variants can be found in approximately 3% of patients with a GS-like tubulopathy.³ Additionally, pathogenic variants in *KCNJ10*, *FXYP2*, and *HNF1B* may result in a similar biochemical phenotype, but typically cause additional symptoms such as sensorineural deafness, epilepsy, ataxia, intellectual disability, diabetes, or renal cysts.^{4–6} Still, 10% of patients with clinical characteristics of GS do not have a pathogenic variant in *SLC12A3* or other genes currently associated with a GS-like tubulopathy, suggesting that not all genetic causes for GS have been identified.³

Mitochondrial diseases form a heterogeneous group of hereditary disorders characterized by mitochondrial dysfunction.⁷ Interestingly, a small group of mitochondrial diseases has been associated with distal tubular dysfunction.^{8–11} For instance, a large family carrying a variant in the mitochondrial transfer RNA (tRNA) (mt-tRNA) gene for isoleucine (*MT-TI*) was affected by hypokalemia and hypomagnesemia in addition to arterial hypertension and hypercholesterolemia.⁹ To date, all reports report extrarenal manifestations in addition to the GS-like electrolyte abnormalities.

In this study, we describe three large families with genetically unexplained GS. The presumed maternal inheritance pattern led to the identification of mitochon-

Significance Statement

Biallelic pathogenic variants in *SLC12A3*, encoding the thiazide-sensitive sodium chloride cotransporter NCC, cause Gitelman syndrome. Gitelman patients suffer from hypokalemic alkalosis, hypomagnesemia, and salt wasting. A subset of Gitelman syndrome cases remains genetically unsolved. This paper describes the identification of pathogenic mitochondrial DNA (mtDNA) variants in the genes encoding the transfer RNAs for phenylalanine (*MT-TF*) and isoleucine (*MT-TI*) in 13 families with a Gitelman-like phenotype. Six families were additionally affected by progressive CKD. Mitochondrial dysfunction was demonstrated in patient-derived fibroblasts and linked to defective sodium reabsorption by NCC *in vitro*. These findings advocate for screening for mtDNA variants in unexplained Gitelman syndrome patients and influence genetic counseling of affected families. Furthermore, they provide insight into the physiology of renal sodium handling.

drial DNA (mtDNA) variants in mt-tRNAs for isoleucine and phenylalanine (encoded by *MT-TI* and *MT-TF*, respectively). We subsequently screened two cohorts of patients with hypomagnesemia or a clinical diagnosis of GS, and identified ten more families with variants in *MT-TI* and *MT-TF*. We analyzed the clinical phenotype of these patients, characterized mitochondrial function in patient-derived fibroblasts, and assessed the effect of mitochondrial dysfunction on NCC-mediated sodium transport.

METHODS

Inclusion and Ethical Approval

The maternal inheritance pattern in families 1, 2, and 3 prompted an analysis of the mitochondrial genome. The identification of three mtDNA candidate variants in *MT-TI* and *MT-TF* encouraged us to screen for variants in these two genes in additional families with unexplained hypomagnesemia or a clinical suspicion of GS (156 families). This led to the identification of variants in *MT-TI* or *MT-TF* in eight more families (families 4–12). Family 13 was known to have a pathogenic variant in *MT-TF* and has been published before as Pedigree III by Connor et al.¹²

The study was performed in accordance with the Declaration of Helsinki, and informed consent was obtained from all patients before inclusion into the study. Where needed, ethical approval was provided by the institutional review board of Arnhem-Nijmegen (study reference 2019–5749).

DNA Sequencing

In family 1, the initial diagnosis was made on DNA isolated from cells in urine, with amplification through long-template PCR and sequencing with the Ion Torrent PGM. The obtained mtDNA sequence was screened for rearrangements and mismatches. The presence of the variant was

Received May 3, 2021. Accepted September 6, 2021.

*The Genomics England Research Consortium members include: John C. Ambrose, Prabhu Arumugam, Roel Bevers, Marta Bleda, Freya Boardman-Pretty, Christopher R. Boustred, Helen Brittain, Mark J. Caulfield, Georgia C. Chan, Greg Elgar, Tom Fowler, Adam Giess, Angela Hamblin, Shirley Henderson, Tim J. P. Hubbard, Rob Jackson, Louise J. Jones, Dalia Kasperaviciute, Melis Kayikci, Athanasios Kousathanas, Lea Lahnstein, Sarah E. A. Leigh, Ivonne U. S. Leong, Javier F. Lopez, Fiona Maleady-Crowe, Merial McEntagart, Federico Minneci, Loukas Moutsianas, Michael Mueller, Nirupa Murugaesu, Anna C. Need, Peter O'Donovan, Chris A. Odhams, Christine Patch, Mariana Buongiorno Pereira, Daniel Perez-Gil, John Pullinger, Tahrima Rahim, Augusto Rendon, Tim Rogers, Kevin Savage, Kushmita Sawant, Richard H. Scott, Afshan Siddiq, Alexander Sieghart, Samuel C. Smith, Alona Sosinsky, Alexander Stuckey, Mélanie Tanguy, Ana Lisa Taylor Tavares, Ellen R. A. Thomas, Simon R. Thompson, Arianna Tucci, Matthew J. Welland, Eleanor Williams, Katarzyna Witkowska, and Suzanne M. Wood.

D.V., K.-P.S., M.H., T.N., R.V.-P., N.K., D.B., and J.B. contributed equally to this work.

Published online ahead of print. Publication date available at www.jasn.org.

Correspondence: Dr. Jeroen H.F. de Baaij, Department of Physiology, Radboud Institute for Molecular Life Sciences, Radboudumc, P.O. Box 9101, 6500HB, Nijmegen, The Netherlands. Email: jeroen.debaaij@radboudumc.nl

Copyright © 2022 by the American Society of Nephrology

later confirmed in DNA isolated from blood by Sanger sequencing using the *MT-TI* sequencing primers listed in Supplemental Table 1. In family 2, DNA was isolated from whole blood. Exome enrichment was done with SureSelectXT Automated Target Enrichment and sequencing by a HiSeq4000 platform (Illumina) with 2×75-bp paired-end reads. Sequence reads were aligned to the Human Genome Reference Assembly GCRh37/hg19 using Burrows-Wheeler Alignment (BWA) version 0.7.12¹³ and indexed using SAMtools version 1.6.¹⁴ SNVs and indels were subsequently called by the Genome Analysis Toolkit (GATK) HaplotypeCaller version 3.4–46. The candidate variant was identified by targeted reanalysis of the mtDNA covered by the exome sequencing data. Family 3 underwent whole-genome 150-bp paired-end sequencing using an Illumina HiSeq X platform as part of the 100,000 Genomes Project, and were processed on the Illumina North Star Version 4 Whole Genome Sequencing Workflow (NSV4, version 2.6.53.23), comprising the iSAAC Aligner (version 03.16.02.19) and Starling Small Variant Caller (version 2.4.7). Samples were aligned to the Homo Sapiens NCBI GRCh38 assembly. The candidate variant was identified after targeted reanalysis of mtDNA. In all three families, results were confirmed by Sanger sequencing in an extended set of family members for segregation (primers are listed in Supplemental Table 1).

Families 4–9 were ascertained through screening for variants in *MT-TI* and *MT-TF* by Sanger sequencing of DNA obtained from whole blood. The variants in families 10 and 12 were identified by analysis of the complete mitochondrial genome with a long-range PCR followed by circular consensus sequencing on a Sequel (Pacific Biosystems). The variant in family 11 was identified by multigene panel analysis (Bioscientia). This multigene tubulopathy panel used Roche/Nimblegen enrichment and sequencing on an Illumina platform. The variant in family 13 was identified by sequencing of the mitochondrial genome.¹² In all families except for family 13, the diagnostic trajectory had included a screen for pathogenic variants in the coding regions of *SLC12A3*, *CLCNKB*, and several other tubulopathy genes by a multigene panel or by exome sequencing.

To exclude other genetic causes of reduced GFR, two genome sequencing panels were analyzed in family 3 (panel names: “unexplained kidney failure in young people” and “tubulointerstitial kidney disease”¹⁵). In family 10, a >300-gene-containing exome sequencing panel for kidney diseases was used. In family 13, targeted genetic analysis of *UMOD*, *HNF1B*, *REN*, and *MUC1* was performed, including SNaPshot minisequencing of *MUC1* and MLPA for *HNF1B* (as described for family 6 in the study by Ekici *et al.*¹⁶).

Determination of Heteroplasmy

Heteroplasmy levels were determined in fibroblasts and/or whole blood from nine families using single-molecule molecular inversion probes. A variant was considered

homoplasmic if coverage at the variant position was at least 300 and the percentage of reads with the variant was >99%. A detailed description can be found in the Supplemental Material.

Identification, Selection, and Assessment of Candidate Variants

Very rare mtDNA variants (population frequency <0.1%) in families 1, 2, and 3 were considered candidate variants. Variant population frequencies were obtained from MITOMAP, HelixMTdb, and gnomAD. Furthermore, MITOTIP and PON-mt-tRNA were used to predict pathogenicity of candidate variants. The secondary structures of the mt-tRNAs for isoleucine (mt-tRNA^{Ile}) and phenylalanine (mt-tRNA^{Phe}) were modeled using rtools, CentroidHomFold. For conservation analysis of *MT-TI* and *MT-TF* (encoding mt-tRNA^{Ile} and mt-tRNA^{Phe}, respectively), we selected the species suggested by Yarham *et al.*¹⁷ and aligned sequences using clustal O followed by manual curation.

Pathogenicity of mtDNA variants was evaluated by using the criteria proposed by Wong *et al.*,¹⁸ similar to the ACGS criteria.¹⁹

Clinical Data

Clinical data, including renal biopsy specimens, were obtained as part of routine clinical care at the respective local centers. Electrolyte measurements were performed in serum samples in some centers, and in plasma samples in others. For simplicity, we will henceforth refer to all as “serum” measurements. Reference values for the measurements presented were very similar across centers. Urinary calcium excretion was normalized to the upper limit of normal to enable comparison between children and adults (Supplemental Table 2). The eGFR was calculated using serum creatinine and the CKD-EPI (adults) or Schwartz formula (children). Hypertension was defined as a systolic BP >140 mm Hg or a diastolic BP >90 mm Hg. In family 12, sexes were left out in some individuals and some unaffected siblings were added for pseudonymization purposes.

Thiazide tests were performed in three families as described in the Supplementary Material, according to previously described protocols.^{20,21}

Fibroblasts

In families 3 and 4, fibroblasts were grown from a skin biopsy sample. In families 6 and 11, fibroblasts were obtained by nasal brush (Cytobrush Plus, Cooper Surgical, #176291). Culture conditions are described in the Supplemental Material. In addition to one family control (unaffected relative on the paternal line in family 6, control 1), two control cell lines of unrelated individuals were included. Both had been shown to have normal mitochondrial function in earlier experiments. One fibroblast line was obtained commercially (ATCC PCS-201–012, lot #61683453, from a 40-year-old woman, control

2); the other was derived from a skin biopsy done at the Radboudumc, Nijmegen (control 3).

Oxidative Phosphorylation Activity Measurements

Measurements of the activity of the mitochondrial oxidative phosphorylation (OXPHOS) complexes were performed per clinical routine as described previously (additional information in the Supplemental Material).²²

Mitochondrial Respiration by the Seahorse XFe96 Analyzer
Oxygen consumption rate (OCR) was measured in a Cell Mito Stress Test by the Seahorse XFe96 Analyzer as described earlier.²³ Citrate synthase activity was measured in all wells after the stress test for normalization purposes (Supplemental Material).

Seahorse XFe96 Data Analysis

Wave Desktop Software version 2.3 (Agilent) was used to read Seahorse data, to remove background signal, and to normalize for citrate synthase activity. However, use of this program for subsequent analysis has several disadvantages. Firstly, there is no automated way to exclude wells that did not respond to the Mito Stress Test (which can occur if one of the drugs was not injected correctly). Secondly, the larger variation observed with larger OCR values (*i.e.*, heteroscedasticity) violates the assumptions underlying many statistical tests, including ANOVA.²⁴ Lastly, interplate variation can be significant.²⁴ To improve the validity of the data, an R-script was developed to analyze the data (Supplemental Material). The code is publicly available on GitHub (<https://github.com/DaanViering/Seahorse-analyzeR>).

Effect of Complex IV Inhibition on NCC-Mediated $^{22}\text{Na}^+$ Uptake

HEK293 cells were transfected with either 0.5 μg of DNA construct containing NCC (pCIneo-NCC-IRES-GFP) or 0.5 μg of construct without NCC (pCIneo-IRES-GFP, hereafter indicated with “mock”). Two days after transfection, samples were put on hypotonic-low-chloride or isotonic buffer with or without 100 $\mu\text{mol/L}$ thiazide, and with either 1 mmol/L potassium cyanide (KCN, experimental condition) or as a control 1 mmol/L potassium chloride (KCl). After half an hour of incubation, samples were put on isotonic buffer containing both $^{22}\text{Na}^+$ and inhibitors of other sodium transporters and channels (*i.e.*, amiloride 100 $\mu\text{mol/L}$, bumetanide 100 $\mu\text{mol/L}$, and ouabain 1 mmol/L). After half an hour in the $^{22}\text{Na}^+$, cells were lysed and radioactivity was measured on a liquid scintillation counter (Hidex 600SL). NCC expression was assessed by immunoblotting, following the same protocol as described below. Culturing and the $^{22}\text{Na}^+$ uptakes were done in triplicate; the complete experiment was performed four times (Supplemental Material).

Effect of Complex IV Inhibition on NCC Phosphorylation

Seeding of HEK293 cells and transfection were similar to what is described above for the $^{22}\text{Na}^+$ uptake experiments. Samples were subsequently put on hypotonic-low-chloride or isotonic buffer with or without 100- $\mu\text{mol/L}$ hydrochlorothiazide, and with either 1-mmol/L KCN (experimental condition) or as a control 1-mmol/L KCl. Culturing was done in duplicate; the complete experiment was performed three times. To investigate the effect of complex IV inhibition on other sodium transporters, its effect on the phosphorylation of the sodium-potassium-chloride cotransporter NKCC2 was assessed using an analogous protocol (Supplemental Material).

Immunoblotting

SDS-PAGE immunoblotting was performed with the following primary antibodies: rabbit anti-NCC (1:2000, Millipore, #AB3553), and rabbit anti-pT58-NCC (NCC phosphorylated at human position p.Thr60, 1:2000, kind gift from Robert Fenton²⁵). Primary antibodies were targeted with the following secondary antibody: peroxidase anti-rabbit-IgG (1:10,000, Sigma Aldrich, #A4914). Imaged blots were subjected to densitometric analysis of band intensities (Supplemental Material).

Statistical Analyses

GraphPad Prism 8.4.3 was used for statistical analyses. For the Seahorse XFe96 experiments, Welch's ANOVA test was applied with the null hypothesis that maximal mitochondrial respiration was not different for any of the variants compared with the control fibroblasts. Correction for multiple testing was performed using Dunnett T3 testing. Additionally, we assessed for each patient whether the maximum mitochondrial respiratory capacity in their fibroblasts was significantly different from the fibroblasts of control 1, again using Welch's ANOVA test (for this, fibroblasts from 5.I.2 were excluded because only one measurement was available) with Dunnett T3 correction.

To assess the difference between the KCN and KCl conditions during the $^{22}\text{Na}^+$ absorption, we used an unpaired *t* test. To assess the difference between the KCN and KCl conditions in the immunoblotting experiments, we used multiple *t* tests with Holm-Sidak correction for multiple testing. Statistical significance was defined as $P < 0.05$ unless stated otherwise.

RESULTS

Identification of Four mtDNA Variants in MT-TI and MT-TF

Three large families with an unexplained GS-like electrolyte constellation showed pedigrees compatible with maternal inheritance (families 1, 2, and 3 in Figure 1). No pathogenic

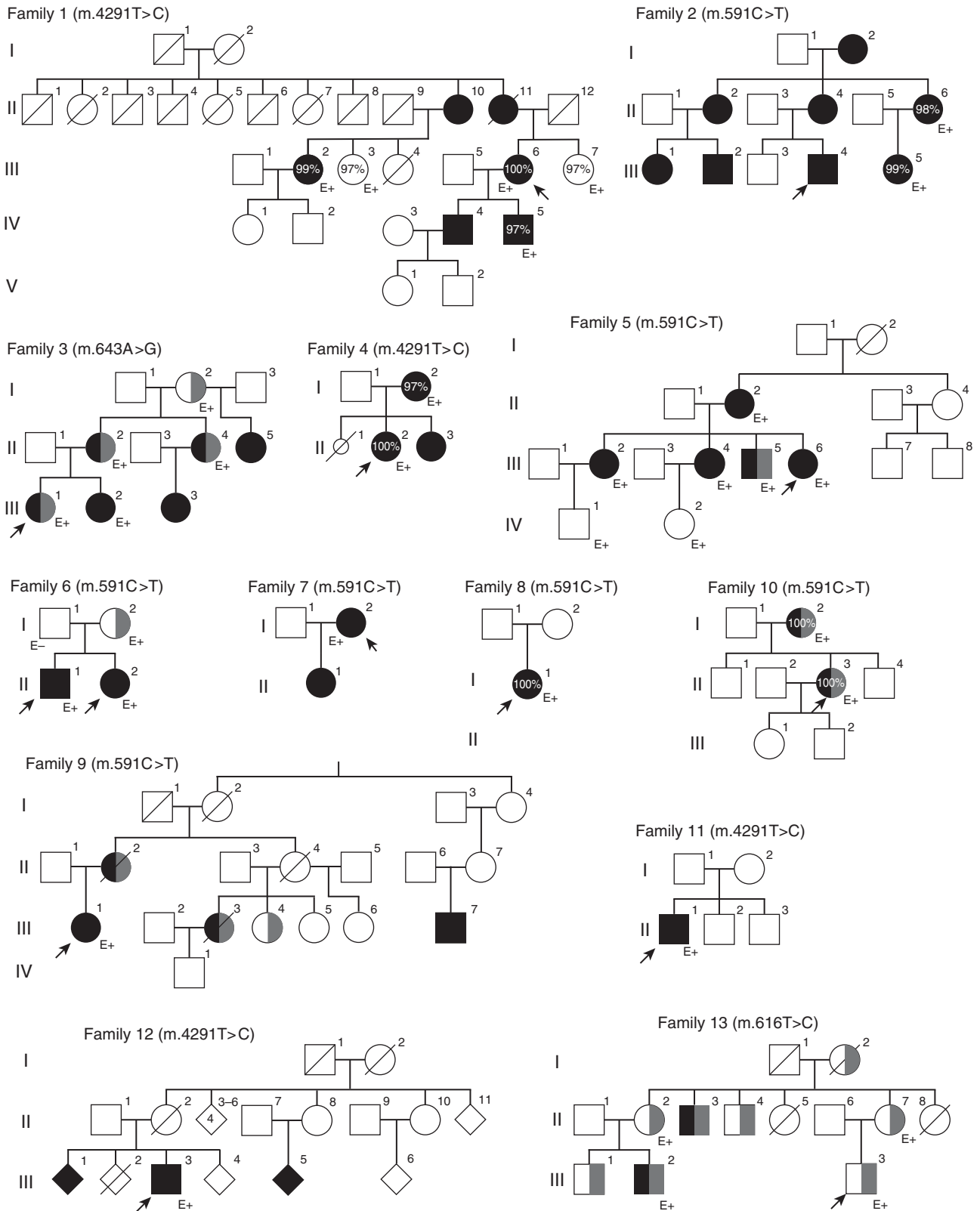


Figure 1. Pedigrees of the 13 affected families demonstrate maternal inheritance pattern. Black filling denotes tubulopathy. Probands are denoted with arrows; CKD (any stage) is denoted by gray filling. Percentages indicate heteroplasmy level of the variant in blood. E+, the presence of the variant as confirmed by genetic testing; E-, the exclusion of the variant.

Table 1. Summary of clinical data

Patient	Sex	Age, ^a yr	Variant	Gene	Heteroplasmy, (% in Blood Fibroblasts)	Serum Magnesium, mmol/L	Fractional Magnesium Excretion	Serum Potassium, mmol/L	eGFR, ml/min per 1.73 m ²	BP, mm Hg	Remarks
Reference range											
1.III.6	F	39	m.4291T>C	MT-TI	100	0.7–1.1 0.40	<4.0 ^b 6.7	3.6–5.2 3.6	>90 82	<140/90 140/80	Primary hyperparathyroidism
1.III.2	F		m.4291T>C	MT-TI	99						
1.IV.4	M	36	m.4291T>C	MT-TI		0.67	2.9	3.7	>90		
1.IV.5	M	34	m.4291T>C	MT-TI	97	0.56	8.3	3.4	>90		
2.II.6	F		m.591C>T	MT-TF	98	0.86 ^c		3.3 ^c	65	122/80	
2.III.1	F	5	m.591C>T	MT-TF		0.73		3.2	>90		
2.III.2	M	10	m.591C>T	MT-TF		0.55	9.0	3.0	>90	125/71	
2.III.4	M	8	m.591C>T	MT-TF		0.71 ^c	13	3.6	>90	151/89	
2.III.5	F		m.591C>T	MT-TF	99	0.48	7.8	3.0	>90	114/65	
3.I.2	F	50	m.643A>G	MT-TF		0.70	7.9	3.6	35		Albuminuria
3.II.2	F	22	m.643A>G	MT-TF		0.52	4.9	3.3	32	120/73	
3.II.4	F	21	m.643A>G	MT-TF		0.66	4.2	3.1	55		
3.II.5	F	14	m.643A>G	MT-TF				2.9			
3.III.1	F	2	m.643A>G	MT-TF		0.76 ^c	8.2	4.1	30	98/54	Albuminuria and elevated RBP. Renal biopsy performed
3.III.2	F	1	m.643A>G	MT-TF		0.48	8.5	3.0	>90		Albuminuria and elevated RBP
3.III.3	F		m.643A>G	MT-TF		0.61		4.3			
4.I.2	F		m.4291T>C	MT-TI	97 100	0.52	4.3	3.4	>90	125/78	
4.II.2	F	15	m.4291T>C	MT-TI	100 100	0.42 ^c	5.3	4.2	>90	113/72	
5.III.6	F	3	m.591C>T	MT-TF		0.10	10.1	3.6	75	123/67	Requires subcutaneous magnesium supplementation. Salt craving
5.II.1	M	70	m.591C>T	MT-TF		0.40		4.9	65		
5.III.2	F	34	m.591C>T	MT-TF		0.40	6.4	3.1	>90	149/91	
5.III.4	F	32	m.591C>T	MT-TF		0.73	2.8	3.7	>90	157/98	
5.III.5	M	42	m.591C>T	MT-TF		0.30	12.1	2.4	77	197/105	
5.IV.1	F		m.591C>T	MT-TF		0.70		3.9	>90	133/80	
5.IV.2	M		m.591C>T	MT-TF		0.80	3	3.9	>90	149/63	
6.I.2	F		m.591C>T	MT-TF					26		Salt and spicy food craving. Salt and spicy food craving.
6.II.1	M	12	m.591C>T	MT-TF		0.44 ^c	9.5	3.1	>90	120/80	High renin and aldosterone
6.II.2	F	10	m.591C>T	MT-TF		0.63 ^c	8.1	3.3 ^c	>90	110/70	Salt and spicy food craving. High renin and aldosterone
7.I.2	F	33	m.591C>T	MT-TF		0.56	5.5	2.8	>90	128/82	High renin and aldosterone

Table 1. Continued

Patient	Sex	Age, ^a yr	Variant	Gene	Heteroplasmy, (% in Blood Fibroblasts	Serum Magnesium, mmol/L	Fractional Magnesium Excretion	Serum Potassium, mmol/L	eGFR, ml/min per 1.73 m ²	BP, mm Hg	Remarks
7.II.1	F	8	m.591C>T	MT-TF		0.74		3.3	>90	101/66	
8.II.1	F	18	m.591C>T	MT-TF	100	0.54 ^c		2.7 ^c		113/65	High renin
9.III.1	F	40	m.591C>T	MT-TF		0.51		4.0 ^c	>90	100/50	Orthostatic hypotension, m. Winiwater–Buerger, migraine, Wolff–Parkinson–White syndrome
10.II.3	F	39	m.591C>T	MT-TF	100	0.59 ^c	5	3.2	50	122/70	Transient mild thrombopenia.
10.I.2	F		m.591C>T	MT-TF		0.68	4	4.5	24		Osteopenia Primary hyperparathyroidism. Mild thrombopenia. CVA (2×). BP controlled with three antihypertensives. Osteopenia
11.II.1	F		m.4291T>C	MT-TI	100	0.52	7.5	3.4 ^c	>90	142/95	
12.II.1	M	46	m.4291T>C	MT-TI		0.56	8.3	4.5	>90		
13.II.3	M	27	m.616T>C	MT-TF		0.54 ^c		4.0	39	120/60	
13.III.2	M	21	m.616T>C	MT-TF		0.60 ^c		3.8 ^c	56		

Summary of clinical data of patients with causative mtDNA variants in MT-TI or MT-TF. If values were outside measurement limits, the value was set equal to the measurement limit. If multiple measurements were available, the first measurement was taken in the case of serum magnesium, serum potassium, and FEMg, whereas the last available measurement was taken in the case of eGFR. eGFR was calculated with CKD-EPI, except for individuals below the age of 19, in which case the Schwartz formula was used. For conversion of serum magnesium (mmol/L) to (mg/dl), multiply by 2.43. FEMg is calculated by: serum creat²×urinary Mg/(serum Mg×urinary creat)×100%.

^aAge at presentation.

^bUpper limit of normal for FEMg applies to hypomagnesemic individuals only and is on the basis of Elisaf et al.⁷⁵

^cWith supplementation of magnesium or potassium.

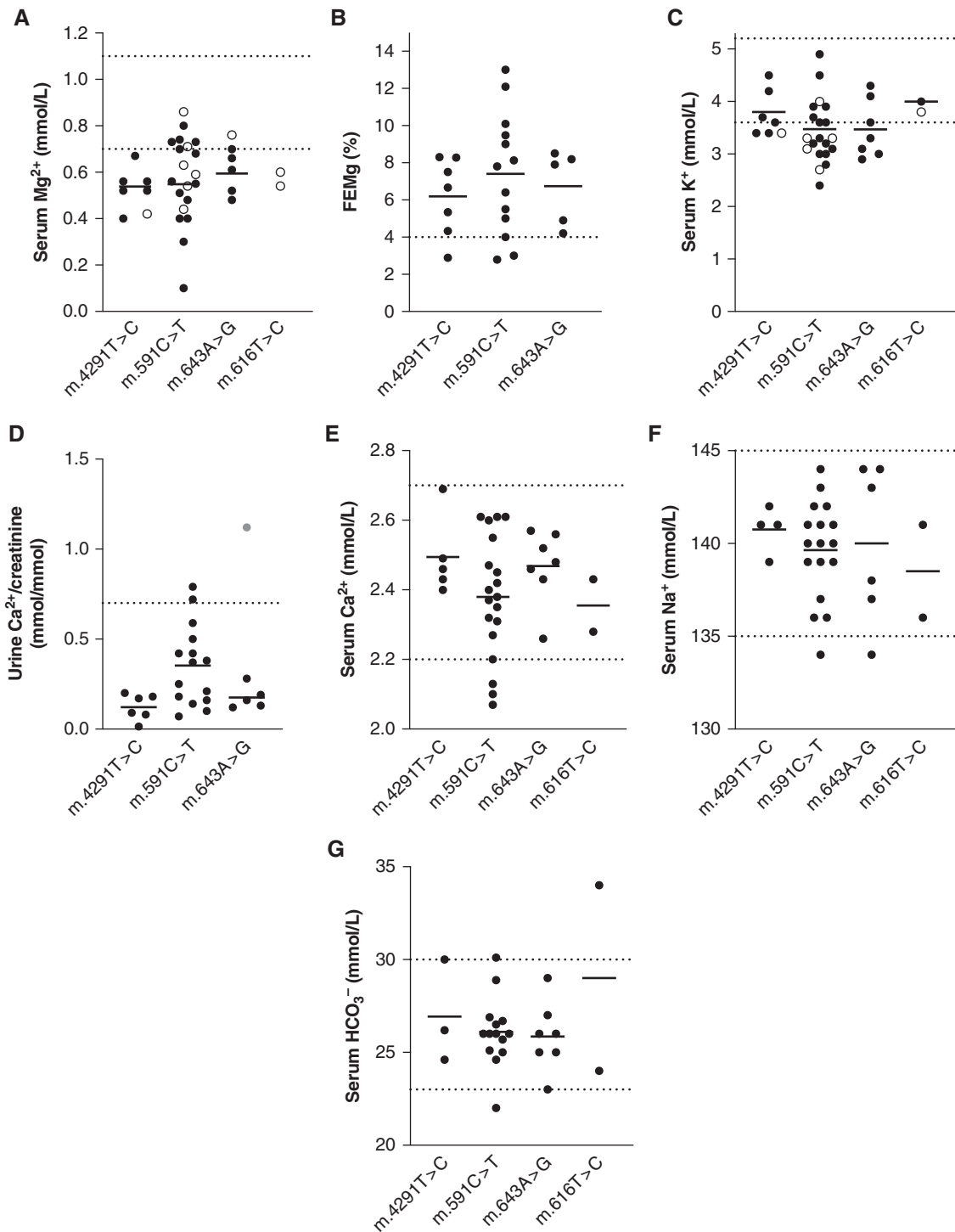


Figure 3. Patients with variants in *MT-TI* or *MT-TF* have Gitelman syndrome-like electrolyte abnormalities. (A–G) Serum and urinary electrolyte values in patients by pathogenic variant. Dotted lines represent upper and lower limits of normal. For the fractional excretion of magnesium (FEMg) and urinary calcium excretion, lower limits of normal were not available; therefore, only the upper limit of normal is depicted in panels (B) and (D). Upper limit of normal for FEMg applies to hypomagnesemic individuals only and these are on the basis of Elisaf *et al.*⁷⁵ Black circles (●), without supplementation; open circles (○), with supplementation; gray circle in panel (D), a child (individual 3.III.2); upper limit of normal for this age is 2.2 mmol/mmol Ca^{2+} /creatinine. FEMg is calculated by: serum creatinine \times urinary magnesium/(serum magnesium \times urinary creatinine) \times 100%.

We subsequently screened for variants in *MT-TF* and *MT-TI* in 156 additional families and individual patients with an unexplained GS phenotype or unexplained hypomagnesemia. This screening identified three more families/individual patients with the m.4291T>C variant and six more families/individual patients with the m.591C>T variant. Lastly, a family with the m.616T>C variant in *MT-TF* (family 13, described previously as “Pedigree III” by Connor *et al.*¹²) was also shown to have GS-like electrolyte abnormalities.

Heteroplasmy levels in blood and fibroblasts ranged from 97% to 100% (homoplasmic) in all tested patients (Table 1, Supplemental Table 3). Pedigrees can be found in Figure 1.

Assessment of Variant Pathogenicity

The m.591C>T, m.616T>C, and m.643A>G variants are all located in the *MT-TF* gene encoding mt-tRNA^{Phe} (Figure 2A). The m.4291T>C variant is positioned in mt-tRNA^{Leu}, encoded by the *MT-TI* gene (Figure 2B). In the MITOMAP Genbank, HelixMTdb, and gnomAD population databases (together comprising 304,824 individuals), homoplasmic occurrences have been observed for the m.643A>G variant (three homoplasmic occurrences, one heteroplasmic occurrence), but not for the other variants (Supplemental Table 4). Furthermore, finding the m.591C>T variant in six of 156 screened families is unlikely to have occurred by chance (corrected *P* value 6.6×10^{-16}). Finding the m.4291T>C variant in three of 156 screened families is also unlikely to have occurred by chance (corrected *P* value 1.7×10^{-9}). Evolutionary conservation ranged from well conserved (m.4291T>C and m.616T>C, conserved to fruit flies) to poorly conserved (m.591C>T, conserved only to chimpanzees), as shown in Figure 2, C and D. Computational evidence was conflicting on pathogenicity of the variants (Supplemental Table 4). Application of the criteria by Wong *et al.*¹⁸ resulted in classification of the m.591C>T, m.616T>C, and m.4291T>C variants as pathogenic and the m.643A>G variant as a variant of uncertain significance (Supplemental Table 5). Variant classifications were submitted to ClinVar.

Clinical Phenotype

To better characterize the clinical phenotype associated with the four variants in *MT-TI* and *MT-TF*, phenotypical data from all patients were collected (Table 1, Figure 3, Supplemental Table 3). Ten index patients presented with hypomagnesemia-related symptoms, such as tetany, tremor, paresthesia, muscle fatigue, joint complaints (chondrocalcinosis), or cerebral seizures at the initial visit. In two other index patients, hypokalemia or hypomagnesemia was discovered as an incidental finding. Of the investigated individuals on the maternal lineage of each family, 31 of 36 had hypomagnesemia (86%). A significant degree of variation in serum magnesium was present among individuals, with patient 5.II.1 having an

immeasurably low serum magnesium (<0.1 mmol/L); she receives supplementation of magnesium with a subcutaneous pump system. A high fractional magnesium excretion in 21 of 25 patients with available data (average 6.9%, range 2.8%–12%) implicated renal magnesium wasting as the cause of the hypomagnesemia. The average serum potassium level was at the lower border of normal (3.5 mmol/L) and hypokalemia was present in 26 of 41 family members on the maternal lineage (63%).

Activation of the renin-angiotensin-aldosterone system is common in GS. In four of eight individuals in whom renin levels were measured, renin was elevated (families 6, 7, and 8). Additionally, aldosterone levels were elevated in two of them. Furthermore, five individuals from families 5, 6, and 9 reported salt and/or spicy food craving.

Increased renal echogenicity was observed in three patients, of whom two had CKD (6.II.1, 3.III.1, and 13.II.3; Supplemental Table 3). Renal ultrasound was unremarkable in three other patients (1.III.6, 6.II.2, 9.II.1, and 13.III.2). One or more renal cysts were present in two patients (10.II.3 and 10.I.2).

Patients with GS have a markedly blunted response to thiazide diuretics.²¹ Thiazide tests were performed in five patients (1.III.6, 4.I.2, 4.II.2, 12.III.3, and 5.II.6). Hydrochlorothiazide (50 mg) induced a maximal increase of fractional chloride excretion (maximal Δ FECI) of 4.39%, 2.52%, 2.38%, 2.35%, and 0.16%, respectively (Supplemental Figure 1). Whereas the first four patients with the m.4291T>C variant (1.III.6, 4.I.2, 4.II.2, 12.III.3) demonstrated a relatively preserved response to hydrochlorothiazide, the response was completely blunted in individual 5.II.6 with the m.591C>T variant (cut-off value used for the diagnosis of GS is 2.3%).²¹

Hypertension was present in eight of 27 individuals (30%), which is comparable to the general adult population.^{27,28}

CKD in Several Families with *MT-TF* Variants

The GFR is usually normal in patients with GS.²⁹ In contrast, a high prevalence of reduced eGFR (eGFR <90 ml/min per 1.73 m²) was observed in six families (families 3, 5, 6, 9, 10, and 13; Table 1, Figure 1, Supplemental Table 3). Interestingly, affected members of all of these families carried a variant in *MT-TF*. Elaborate screening for other genetic causes of reduced GFR by different gene panels was negative in tested families (families 3, 10, and 13).

In family 3 (m.643A>G), eGFR was impaired in four individuals (median eGFR 34 ml/min per 1.73 m², ranging 30–55). The only individual in this family with a currently normal eGFR (100 ml/min per 1.73 m²) was a 2-year-old girl (3.III.2). The older sibling (3.III.1) developed ESKD necessitating kidney transplantation at the age of 9 years. We observed mild albuminuria (8–22.7 mg/mmol creatinine) in three patients (3.II.2, 3.III.1, and 3.III.2). In family 5, a mild decrease in eGFR was observed in three individuals (5.II.1, 5.III.5, and 5.III.6; eGFR between 60 and 90 ml/

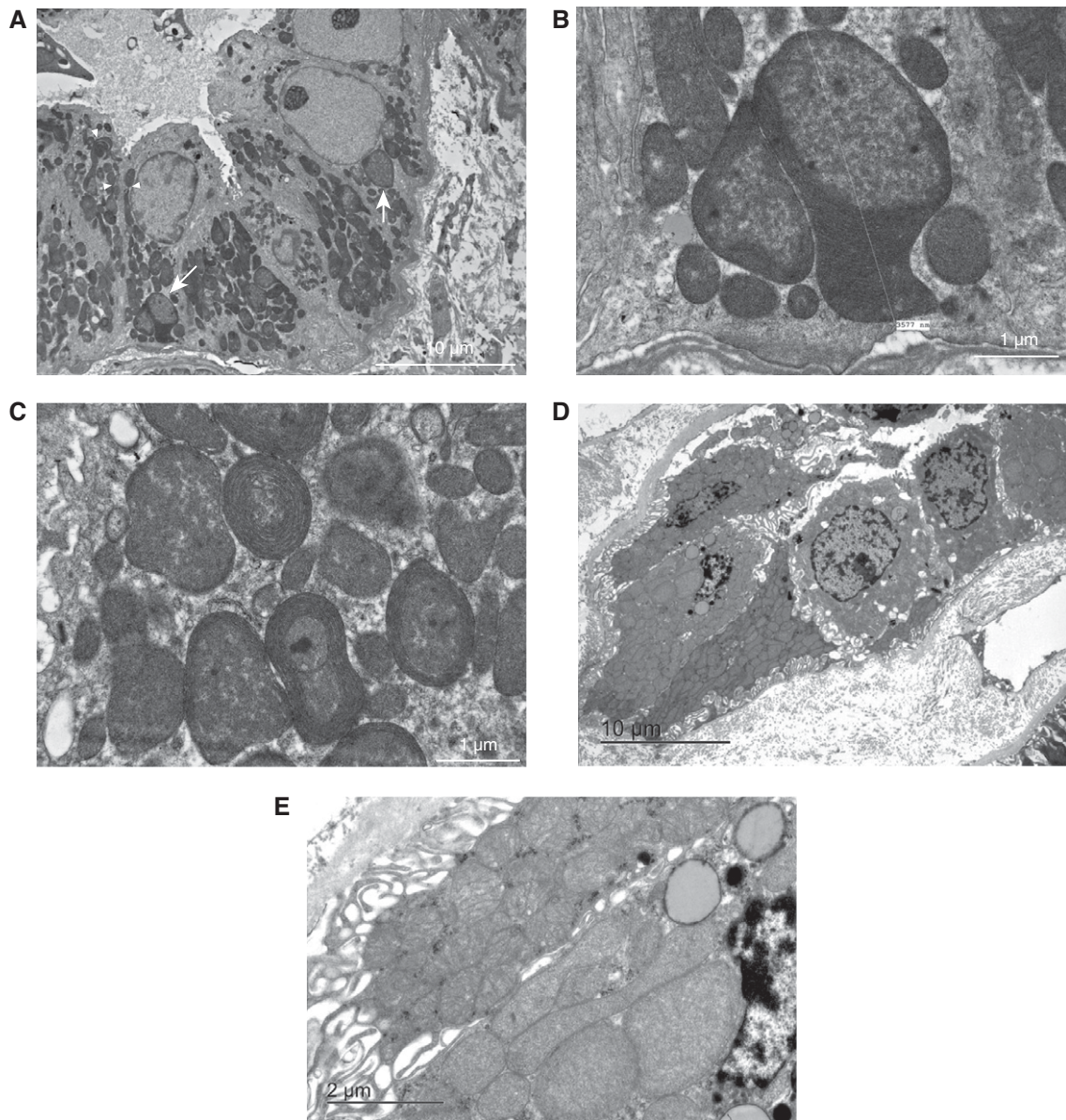


Figure 4. Renal biopsies of two *MT-TF* patients show abnormal mitochondria in distal parts of the nephron. (A–C) Transmission electron microscopy of the renal biopsy sample of patient 3.III.1. (D and E) Transmission electron microscopy of a percutaneous renal biopsy sample of patient 10.II.3. (A) Representative image of a perpendicular cross-section of the distal tubule, with a large number of abnormally shaped and sized mitochondria (two examples indicated with white arrows). Cristae profiles appear distorted, including some mitochondria with no discernable cristae. Nanotunneling visible (three examples indicated with white arrowheads). Magnification, $\times 1000$. (B) Close-up of atypical giant mitochondrion of $>3 \mu\text{m}$ in length (same as indicated by the left arrow in panel [A]). Note the large size and compartmentalization. Magnification, $\times 6000$. (C) Close-up of atypical mitochondria (not in panel [A]). Note the concentric cristae (onion-like appearance). Magnification, $\times 6000$. (D) Representative image of a perpendicular cross-section of the distal tubule; enlarged mitochondria are visible. (E) A close-up of panel (D) shows an almost complete lack of cristae structure in most mitochondria.

min per 1.73 m^2). In family 6, individual 6.I.2 had reached CKD stage 4 (eGFR 15–30 ml/min per 1.73 m^2) at the time of study, and she reported having a sister diagnosed with CKD and early onset diabetes. On the basis of a family history in family 9, three individuals were affected by CKD, of whom 9.III.3 is on hemodialysis and 9.III.4 has received

her second kidney transplantation. Individuals 10.I.2 and 10.II.3 had an eGFR of 24 and 50 ml/min per 1.73 m^2 , respectively. Lastly, family 13 (m.616T>C) was diagnosed initially with autosomal dominant tubulointerstitial kidney disease¹² on the basis of a KDIGO consensus report.³⁰ Data were available for ten individuals in the maternal lineage.

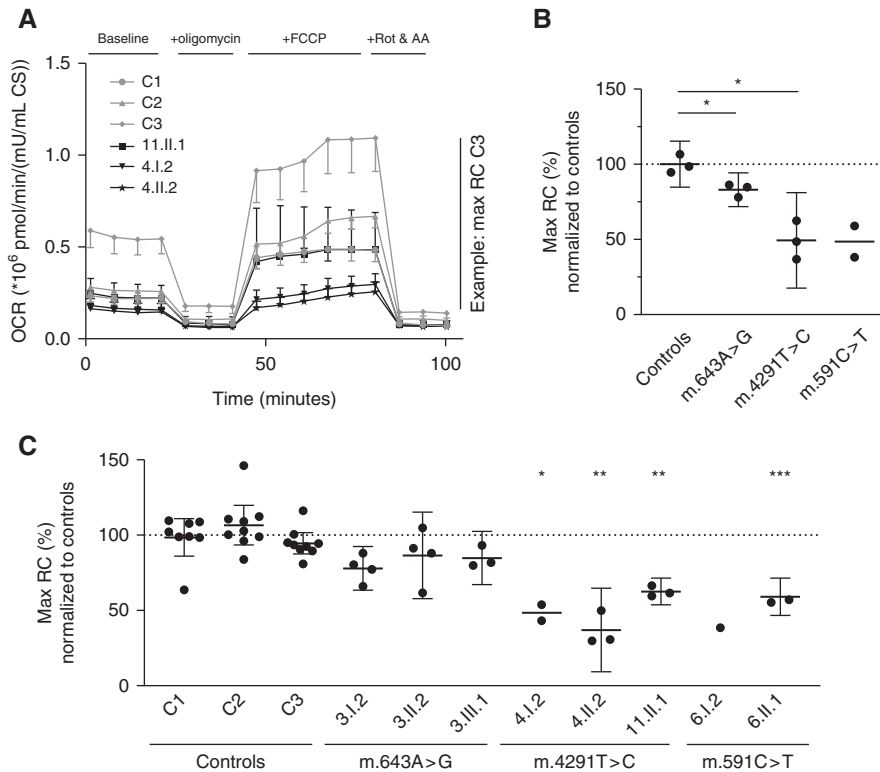


Figure 5. Mitochondrial maximal respiratory capacity is reduced in patient fibroblasts. Mitochondrial function assessed by the Seahorse XFe96 analyzer. (A) Representative OCR plot of a Mito Stress Test of fibroblasts from three patients with the m.4291T>C variant and three controls ($n=6$ wells for each measurement point). Error bars denote \pm SD. (B) Average maximal mitochondrial respiration for the different mtDNA variants. Each point represents the average of all independent experiments for one individual ($n=1-9$, depending on the individual, as can be seen in panel [C]). (C) Average maximal mitochondrial respiration for each individual. Each point represents the average of all replicate wells on one Seahorse plate ($n=6$). (B and C) Means are represented by horizontal bars, error bars denote the 95% confidence interval, and a one-way ANOVA with Dunnett T3 was used to calculate significance. OCR is in $\text{pmol O}_2/\text{min}$ per mU/ml citrate synthase. AA, antimycin A; CS, citrate synthase activity; FCCP, carbonyl cyanide 4-(trifluoromethoxy)phenylhydrazone; RC, respiratory capacity; Rot, rotenone. * $P<0.05$; ** $P<0.005$; *** $P<0.0005$.

Eight had a decreased eGFR, of whom two are included in this study on the basis of their electrolyte abnormalities. Four of these eight individuals currently receive RRT.

Kidney biopsy specimens have been taken in families 3, 10, and 13. The kidney biopsy performed in patient 3.III.1 to investigate CKD showed localized cortical scarring with tubular atrophy, glomerulosclerosis, interstitial fibrosis, and a chronic interstitial infiltrate. After identification of the m.643A>G variant in this individual, electron microscopy was performed and showed abnormal mitochondria, especially in the distal tubule (Figure 4, A–C). Notably, proximal convoluted tubules demonstrated well-developed apical microvilli and normal mitochondria. Other cells, including blood vessel smooth muscle and endothelial cells, showed no apparent mitochondrial irregularity. The kidney biopsy specimen of patient 10.II.3 contained sclerosed glomeruli (20%) together with interstitial fibrosis and tubular atrophy (10%). Examination of the distal tubule by electron microscopy showed evidently abnormal mitochondria (Figure 4, D and E). In this patient, mitochondria appeared abnormal in both proximal

tubule and distal tubule, although mitochondria in proximal tubules had better cristae structures than those in the distal tubule (Supplemental Figure 2, A and B). In this patient, electron microscopy also showed subtle signs resembling those normally seen in chronic thrombotic microangiopathy. Kidney biopsy specimens in family 13 showed isolated interstitial fibrosis with tubular atrophy. Unfortunately, biopsy samples and images could not be retrieved for this family as they were taken several decades ago.

Apparent Absence of Extrarenal Disease

In contrast to patients with other mitochondrial diseases, serum lactate was normal in all patients who were tested. Furthermore, no signs of proximal tubular disease were seen, because urinary amino acid analyses were unremarkable in the seven patients tested (families 3 and 6). Proteinuria was absent in the tested healthy individuals (seven patients from families 2, 4, 5, 7, 11, and 12), but was present in 10.II.3. Newcastle Mitochondrial Disease Adult Scale scores were low and

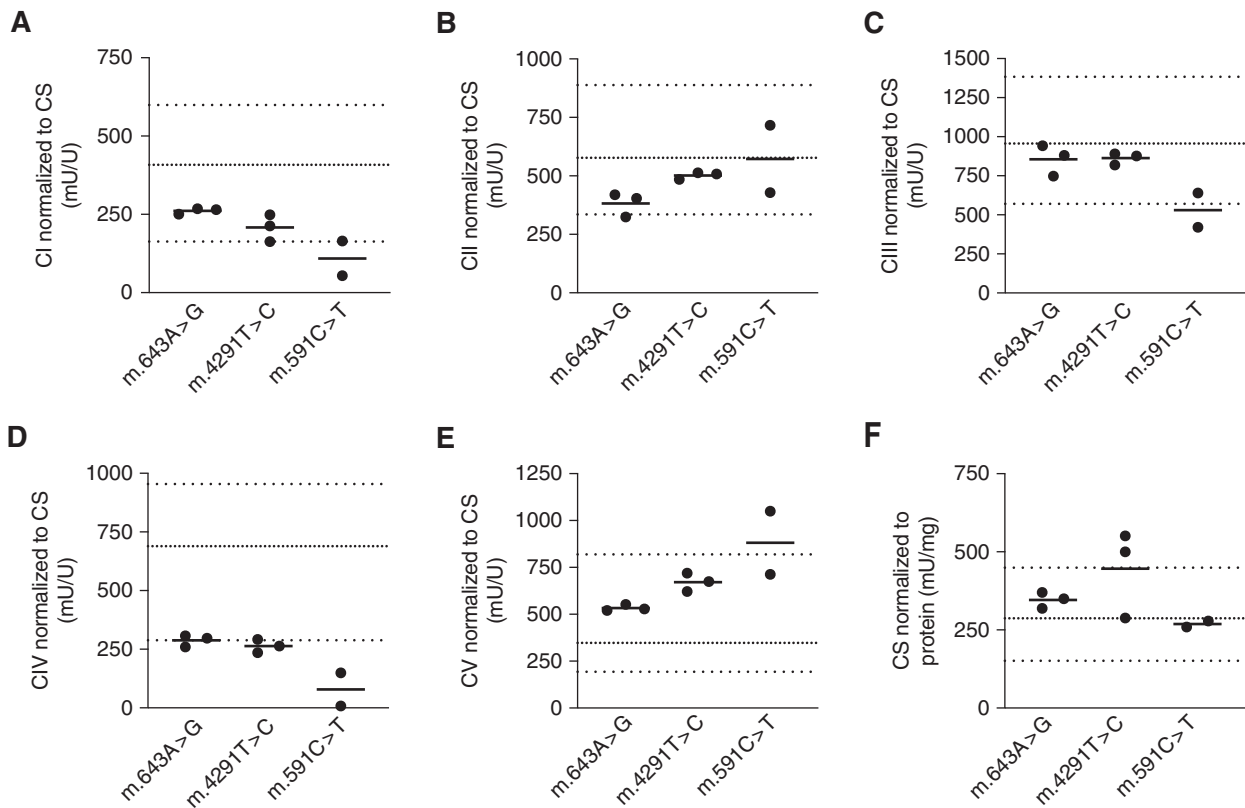


Figure 6. OXPHOS complex IV activity is reduced in patient mitochondria. (A–E) Activities of the five OXPHOS complexes (CI–CV), and (F) citrate synthase activity. All measurements were performed in isolated mitochondria from patient-derived fibroblasts. Thick, dotted lines represent the reference range from our center; thin, dotted lines represent the means of control individuals. CI to CV, OXPHOS complexes I to V; CS, citrate synthase activity.

would concur with calling the two patients “asymptomatic” (4.I.2 and 4.II.1). No obvious abnormalities were seen on cholesterol levels (total cholesterol, HDL, and LDL; Supplemental Table 3).

Mitochondrial Function in Fibroblasts

To confirm that the mtDNA variants are indeed associated with mitochondrial dysfunction, we isolated fibroblasts from eight patients and assessed mitochondrial function. The Mito Stress Test on a Seahorse XFe96 (Figure 5A) showed decreased maximal mitochondrial respiration in fibroblasts from patients compared with controls (Figure 5B). The average decreases for the respective mutants were: a 17% decrease for m.643A>G ($P=0.046$), a 51% decrease for m.4291T>C ($P=0.02$), and a 51% decrease for m.591C>T (not significant, $P=0.22$). Welch’s ANOVA showed a significant difference between all individuals ($P<0.0001$), with a Dunnett T3 test showing that the maximal respiratory capacity in fibroblasts of 6.II.1, 4.I.2, 1.II.2, and 11.II.1 differed significantly from maximal respiratory capacity in control 1 (corresponding to the unaffected father, 6.I.1; Figure 5C).

We hypothesized that the defect in mitochondrial respiration would be caused by dysfunction of one or more

OXPHOS complexes, and measured their activity. Patient fibroblasts showed an average 67% reduction in the activity of OXPHOS complex IV (also known as cytochrome C oxidase) compared with reference values of healthy individuals (Figure 6D). The individual with the greatest reduction in maximal mitochondrial respiration also showed the largest impairment in complex IV activity (6.I.2). OXPHOS complex I activity was low to borderline normal in patients 6.I.2, 6.II.2, and 11.II.1 (Figure 6A). Activity of OXPHOS complexes II, III, and V was within the reference range in all patients, except for patients 6.I.2 and 3.II.1 (Figure 6, B, C, and E). Citrate synthase activity was within the reference ranges in all patients, except for individuals 4.I.2 and 4.II.2 (m.4291T>C), who had elevated activity (11% and 23% above the upper boundary of normal; Figure 6F).

Complex IV does not have a particularly high content of phenylalanine and isoleucine, as can be seen in Supplemental Table 6.

Complex IV Inhibition Reduces NCC-Mediated Sodium Absorption in HEK293 Cells

Because of the clinical similarities with GS and the abnormal mitochondria in the distal tubule observed with electron

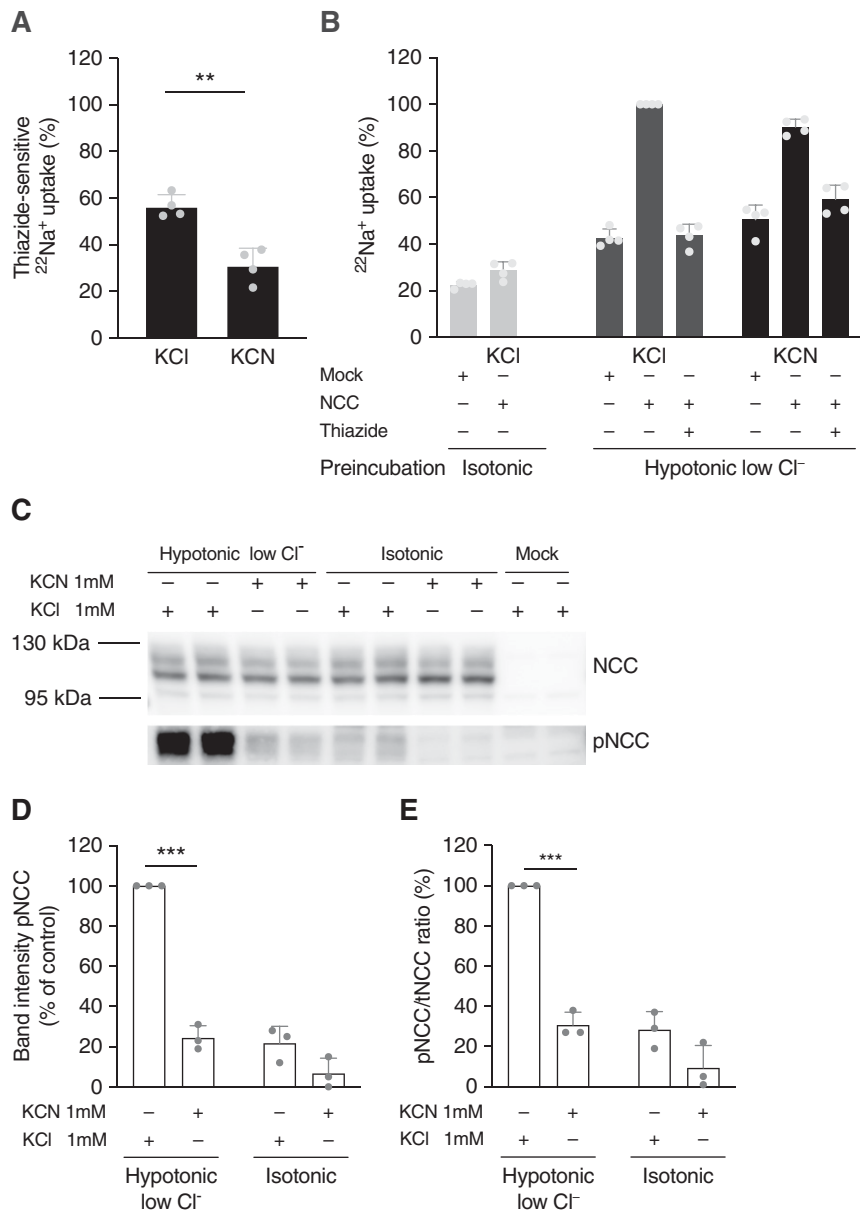


Figure 7. NCC-mediated sodium uptake and NCC-phosphorylation are reduced with complex IV inhibition. (A and B) $^{22}\text{Na}^+$ uptake in HEK293 cells transfected with NCC or mock, with or without inhibition of OXPHOS complex IV with KCN. KCN 1 mmol/L or KCl 1 mmol/L (control) was added during both preincubation and the uptake period, as indicated; the same applies to hydrochlorothiazide (HCTZ) 100 $\mu\text{mol/L}$. Bars represent mean with SD. (A) HCTZ-sensitive $^{22}\text{Na}^+$ uptake of NCC-transfected cells over a period of 30 minutes. Data in (A) are on the basis of (B). Significance was assessed with an unpaired *t* test. (B) $^{22}\text{Na}^+$ uptake in 30 minutes after preincubation with hypotonic-low-chloride buffer or isotonic buffer. Cells were transfected with NCC or mock and treated with KCl or KCN ($n=4$ of triplicates in each experiment). (C) Representative immunoblots showing NCC and phosphorylated NCC after a 30-minute incubation in hypotonic-low-chloride or isotonic buffer, with either KCN or KCl treatment. The mock condition has been incubated in hypotonic-low-chloride buffer as well. (D–E) Densitometry analysis of pNCC band intensity, and pNCC/tNCC ratio ($n=3$ duplicates in each experiment). Significance was assessed with unpaired *t* tests and corrected for multiple testing. pNCC, NCC phosphorylated at Thr60. ** $P<0.005$; **** $P<0.00005$.

microscopy, we hypothesized that inhibition of OXPHOS complex IV would reduce NCC-mediated sodium uptake. Indeed, inhibition of complex IV with the specific inhibitor^{31,32} KCN reduced thiazide-sensitive $^{22}\text{Na}^+$ absorption in

NCC-transfected HEK293 cells by 45% ($P=0.001$; Figure 7A, Supplemental Figure 3). Even when adjusting for the observation that KCN induced an increase in $^{22}\text{Na}^+$ uptake in mock-transfected cells and hydrochlorothiazide-treated cells, KCN

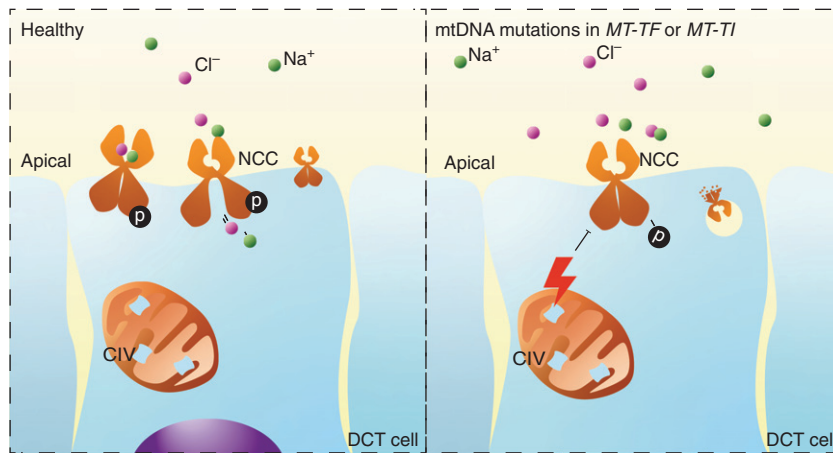


Figure 8. Induction of Gitelman-like syndrome by pathogenic mtDNA variants, proposed mechanism. Proposed mechanism of Gitelman-like syndrome induced by pathogenic mtDNA variants in the genes encoding the isoleucine and phenylalanine tRNAs (*MT-TI* and *MT-TF*, respectively). The m.4291T>C, m.591C>T, m.616T>C, and m.643A>G variants lead to complex IV dysfunction and reduced maximal respiration. This leads to a decrease in the phosphorylation of NCC and sodium transport. Reduced sodium transport in the DCT leads to reduced magnesium transport in the DCT and increased sodium transport in the collecting duct. Increased sodium reabsorption in the collecting duct leads to increased potassium excretion through ROMK (not shown here). CIV, OXPHOS complex IV.

still reduced $^{22}\text{Na}^+$ uptake by 10% (Figure 7B). Furthermore, KCN blunted the response on NCC phosphorylation that is normally observed after 30 minutes of incubation in hypotonic-low-chloride buffer (adjusted $P=0.00006$; Figure 7, C–E, Supplemental Figure 4). A similar effect was observed for KCN on NKCC2 phosphorylation in hypotonic-low-chloride buffer ($P=0.007$; Supplemental Figures 5 and 6).

DISCUSSION

To date, approximately 10% of cases with clinical characteristics of GS remain genetically unsolved.³ Here, we show that variants in two mt-tRNAs can lead to a GS-like syndrome, even in the apparent absence of other manifestations of mitochondrial disease. Thirteen families are described with hypokalemia and hypomagnesemia caused by renal magnesium wasting together with elevated renin levels. Nine families carry a variant in *MT-TF*, which encodes the mt-tRNA for phenylalanine. Four families carry a variant in *MT-TI*, encoding the tRNA for isoleucine. The variants in *MT-TF* were associated with the development of CKD in 19 individuals on the maternal lineage of six families. Electron microscopy of kidney biopsy specimens from two individuals with a pathogenic variant in *MT-TF* and CKD demonstrated tubulointerstitial kidney disease and abnormal mitochondria in the distal tubule. Cells in the DCT have the largest number of mitochondria per unit length of the nephron and would therefore be sensitive to mitochondrial dysfunction.³³ In line with these findings, patient-derived fibroblasts were found to exhibit a disturbed mitochondrial OXPHOS, putatively caused by a

significant impairment of complex IV that was observed in patient mitochondria. In HEK293 cells, pharmacologic inhibition of complex IV was shown to result in a reduction in NCC-mediated sodium reabsorption. We propose that the mitochondrial variants result in reduced NCC activity (Figure 8).

In total, we identified three different variants in *MT-TF* in nine families, of which m.591C>T has not been described before, and describe the m.4291T>C variant in *MT-TI* in three other families. Heteroplasmy levels ranged from 97% to 100% (homoplasmy) in all affected individuals, suggesting that a large proportion of mtDNA copies needs to be affected before a clinically overt phenotype manifests itself.

The four mtDNA variants described here were associated with hypomagnesemia, hypokalemia, and activation of renin production, hallmarks of GS.⁹ Two other symptoms of GS, hypocalciuria and metabolic alkalosis, were only ascertained in a subset of patients. Interestingly, none of the 13 families had clinically overt extrarenal manifestations of mitochondrial dysfunction at the moment of this study. This is in contrast to what is normally observed with pathogenic variants in mtDNA or nuclear-encoded mitochondrial genes.^{8–10,34} Systematic evaluation of symptoms associated with mitochondrial dysfunction should be performed to definitively exclude the presence of rare or subclinical extrarenal manifestations. Yet, specific mtDNA variants have been described that can result in diseases that affect only a single organ, such as in Leber hereditary optic neuropathy and nonsyndromic hearing loss.⁷ Our results show that mt-tRNA variants can cause a maternally inherited GS-like syndrome. Moreover, mt-tRNA variants may

explain other familial and sporadic individual cases, because systematic screening of our cohort identified pathogenic mtDNA variants in nine of 156 families with characteristics of GS.

Genetic heterogeneity and pleiotropy are common phenomena in mitochondrial disorders. For example, the MELAS phenotype (mitochondrial encephalomyopathy, lactic acidosis, and stroke-like episodes) can be caused by pathogenic variants in the mt-tRNA for leucine (*MT-TL1*), phenylalanine (*MT-TF*), and histidine (*MT-TH*).^{35–37} On the other hand, different pathogenic variants in one mt-tRNA can lead to different clinical manifestations. For instance, variants in *MT-TI* and *MT-TF* have already been associated with cardiomyopathy,³⁸ Leigh syndrome,³⁹ non-syndromic hearing loss,⁴⁰ chronic progressive external ophthalmoplegia,⁴¹ and MELAS.³⁵

The specific base pair affected by the variant thus appears to be important, as demonstrated by the finding of multiple families with the m.591C>T and m.4291T>C variants in our study. Interestingly, variants in *MT-TF* have previously been associated with renal phenotypes, especially tubulointerstitial kidney disease with progressive kidney failure.^{12,42–45} Indeed, also in our cohort, CKD was observed in affected members of two families with the m.643A>G and m.616T>C variants and members of four of the seven families with the m.591C>T variant (all in *MT-TF*). In contrast, CKD is not a hallmark of classic GS, nor did any of the patients with the m.4291T>C variant (affecting *MT-TI*) have CKD. Thus, the different mtDNA variants might confer a varying predisposition to tubulointerstitial kidney disease and loss of GFR.

The clinical similarity with GS and the finding of abnormal mitochondria in the distal tubule on a renal biopsy specimen suggested that the mitochondrial dysfunction reported here is responsible for a defect in sodium and magnesium reabsorption in this tubular segment. The electrolyte abnormalities in GS are caused by loss of function of NCC, the electroneutral sodium-chloride cotransporter expressed apically in the DCT. Notably, other genetic diseases have further highlighted the link between reduced NCC function and GS-like electrolyte abnormalities.^{46–48} For instance, pathogenic variants in three DCT-localized proteins, namely ClC-Kb (*CLCNKB*), Kir4.1 (*KCNJ10*), and Kir5.1 (*KCNJ16*), give rise to very similar electrolyte abnormalities as observed in GS.^{49–51} Kir4.1 is essential for K⁺ extrusion at the basolateral membrane and for recycling K⁺ imported by the Na⁺-K⁺-ATPase.⁴⁹ Loss of function of Kir4.1 thus reduces basolateral negative membrane potential.⁵² This inhibits Cl⁻ extrusion through ClC-Kb, a basolateral chloride channel encoded by *CLCNKB*.⁵³ A subsequent rise in intracellular chloride is sensed by WNK4 and thus reduces activation of SPAK/OSR1.^{54,55} Finally, this will lower NCC phosphorylation and consequently NCC-mediated sodium transport.⁵⁶

Here, we provide evidence that pathogenic variants in *MT-TI* and *MT-TF* also impair NCC function. Patient-derived fibroblasts showed impairment of mitochondrial function, especially of OXPHOS complex IV. Given the difficulty of introducing mtDNA mutations in a cell model, we decided to take a pharmacologic approach at inhibiting complex IV. This indeed resulted in lower NCC phosphorylation and lower NCC-mediated sodium transport.

Reabsorption of sodium is a process with a high energy demand, and even more so in the DCT because of the smaller osmotic gradient.⁵⁷ To accomplish this, the DCT is dependent on aerobic energy production.^{58–60} Consequently, mitochondrial dysfunction here might lead to diminished function of the Na⁺-K⁺-ATPase, which needs ATP to maintain basolateral membrane potential, a prerequisite for sodium and magnesium transport.^{61,62} Supporting this mechanism, pathogenic variants in *FXYD2*, *ATP1A1*, and *HNF1B* are also known to cause a GS-like phenotype.^{5,63–66} *FXYD2* and *ATP1A1* encode two different subunits of the Na⁺-K⁺-ATPase, whereas *HNF1B* has been shown to regulate *FXYD2* and *KCNJ16* mRNA expression.^{67,68}

Whereas one patient showed a blunted response to the administration of hydrochlorothiazide, three patients demonstrated a larger increase in maximal Δ FECI than observed in patients with GS, suggesting residual NCC function in these patients. This is in line with other GS-like tubulopathies, such as those caused by pathogenic variants in *CLCNKB* or *HNF1B*. In these patients also, thiazide tests did not show the same level of reduction in thiazide response as has been established for GS.^{21,69,70}

The penetrance of hypocalciuria is lower in our patients than in GS. Interestingly, urinary calcium excretion in *CLCNKB* patients, *HNF1B* patients, and *FXYD2* patients does not seem to be as low as in GS, either.^{65,66,71} Metabolic alkalosis seems to be more pronounced in classic GS, too.^{65,66} For these diseases, it is thought that the phenotypic differences arise from an additional dysfunction of other segments, e.g., thick ascending limb dysfunction in *CLCNKB*, in addition to the effects in the DCT. We cannot exclude that *MT-TI/MT-TF*-associated GS-like syndrome also affects the connecting tubule^{72,73} or the thick ascending limb. Indeed, our *in vitro* data demonstrate reduced NKCC2 phosphorylation.

The m.4291T>C variant has been reported before in a large family with a 50% penetrance of hypertension, hypercholesterolemia, and hypomagnesemia,⁹ and in a family with congenital cataract.⁷⁴ In the 13 families with an mtDNA variant reported here, no individuals were affected by congenital cataract. Hypercholesterolemia and hypertension were not more frequent than in the general population, although this conclusion might not be generalizable to all four variants. Incomplete penetrance of clinically significant hypomagnesemia was noticed in a few cases too, even with (near) homoplasmic presence of the variant, although

we cannot exclude the presence of subclinical symptoms. Systematic analysis of a larger number of patients and families will be required to identify subclinical symptoms and determine the penetrance of additional disease manifestations in the different variants. The m.616T>C variant has been reported before in three families,^{12,44,45} but none of these had reported GS-like electrolyte abnormalities. However, it should be noted that these symptoms could have been missed initially, as in family 13, or could develop later in life.¹²

The m.643A>G variant has been reported only once before,¹⁸ and was classified in this study as a variant of uncertain significance toward the pathogenic side of the spectrum.¹⁹ Future studies might provide decisive evidence on its pathogenicity.

Current next-generation sequencing analyses usually do not report mitochondrial variants. Not all exome sequencing kits cover the mitochondrial genome well, and if they provide adequate coverage, pipelines often focus on variants in or near protein coding sequences in nuclear DNA. Nevertheless, identification of pathogenic near homoplasmic mtDNA variants has important clinical and genetic implications. First of all, clinicians should be aware of the combination of GS-like electrolyte abnormalities and progressive CKD in patients with *MT-TF* variants. Secondly, our findings stress that clinicians treating patients with mitochondrial disorders should appreciate the possibility of electrolyte abnormalities, because hypomagnesemia might sometimes explain part of the muscle complaints. Furthermore, finding mtDNA variants in patients with unexplained GS has important consequences for genetic counseling, given the different inheritance pattern. Thus, specific testing for pathogenic variants in the mitochondrial genome, or including the mitochondrial genome in analyses of next-generation sequencing approaches, is warranted. Lastly, the fact that the variant was found in (near) homoplasmic state in all families suggests that genetic testing can be performed on DNA isolated from blood (in contrast to many other mitochondrial disorders, where affected tissue is needed to avoid false negative results).

In conclusion, *MT-TI* and *MT-TF* variants can cause a Gitelman-like syndrome. In all patients evaluated for a genetic cause of hypomagnesemia or hypokalemia, clinicians should consider screening *MT-TI* and *MT-TF* for pathogenic variants by next-generation sequencing or specific mtDNA testing. Importantly, pathogenic variants in *MT-TF* also confer a significant risk for the development of CKD.

DISCLOSURES

C. Bergmann reports Ownership Interest in Medizinische Genetik Mainz; Research Funding from Limbach; Honoraria from Alexion, Athenium, Kyowa Kirin, Merck, Otsuka, PTC, Sanofi; Scientific Advisor or Membership via medical and scientific board of German PKD Foundation,

advisory boards of PTC, and Alexion; and Other Interests/Relationships as member of the kidney community (GPN, DGIN, ERA/EDTA, IPNA, ESPN, ASN). D. Bockenhauer reports Consultancy Agreements with Advicenne, Avrobio, Otsuka, Sanofi; Honoraria from Advicenne, Recordati; and Scientific Advisor or Membership as associate editor of *Pediatric Nephrology*, *NDT*, and editorial board of *JASN*. P. Houillier reports Consultancy Agreements with Amgen, Shire/Takeda, KyowaKirin; Research Funding from Amgen, Takeda/Shire; Honoraria from KyowaKirin, Takeda/Shire; Scientific Advisor or Membership with NCCR Kidney.CH (Switzerland); Member of the editorial board of *JASN*; and Other Interests/Relationships via working group on calcium and bone for the European Society of Endocrinology. G. Klaus reports Consultancy Agreements: Fresenius Medical Care as Oral presentation at ESPN 2021, Vifor Fresenius Medical Care Renal Pharma Ltd (stopped 2020); Honoraria from Fresenius Medical Care for Oral presentation at ESPN 2021, Vifor Fresenius Medical Care Renal Pharma Ltd (stopped 2020); Other Interests/Relationships with KfH-Kuratorium für Dialyse und Nierentransplantation, and Gesellschaft für Pädiatrische Nephrologie (GPN) Speaker for medical education. N. Knoers reports Honoraria from ErasmusMC, The Netherlands, for SEP evaluation; Scientific Advisor or Membership via different research advisory committees without any financial compensation; and Other Interests/Relationships as Chair board ERA-EDTA WGIKD, Chair Task Force Molecular Diagnostics, European Reference Network of Rare Renal Diseases, ERKNET. M. Konrad reports Consultancy Agreements with Otsuka. A. Mallett reports Research Funding from Otsuka, Sanofi-Genzyme; Scientific Advisor or Membership with Otsuka; Other Interests/Relationships as Local Site Trial Investigator for Achillion, Dicerna, Novotech, Reata, Sanofi-Genzyme; and Research Fellowships with RACP Jacquot Research Establishment Fellowship and MNHHS Clinical Research Fellowship. T. Nijenhuis reports Research Funding from the Dutch Kidney Foundation, Radboudumc; Scientific Advisor or Membership via Scientific board of the Dutch Society for Nephrology, Scientific advisory board of the Dutch Kidney Foundation, Co-chair of the Tubulopathies Expert Working Group, European Rare Kidney Disorders Network (ERKNet), and Board member of ERA-EDTA Working Group Inherited Kidney Disorders. A. van Eerde reports Other Interests/Relationships with ERA-EDTA, Working Group Inherited Kidney Diseases Board, ERKNet, WG chair receives funding from the Dutch Kidney Foundation. R. Vargas-Poussou reports Scientific Advisor or Membership with Advicenne. J. de Baaij reports Research Funding from the Dutch Kidney Foundation and the Dutch Diabetes Research Foundation. All remaining authors have nothing to disclose.

FUNDING

This work was financially supported by the IMAGEN project which is cofunded by the PPP Allowance made available by Health~Holland, Top Sector Life Sciences & Health, to stimulate public-private partnerships (Implementation of Advancements in GENetic Kidney Disease, LSHM20009) and the Dutch Kidney Foundation (Nierstichting) (20OP+018). Additionally, we received support from ZonMW under the frame of EJPRD, the European Joint Programme on Rare Diseases (EJPRD2019-40). This project has received funding from the European Union's Horizon 2020 Research and Innovation Programme under the EJP RD COFUND-EJP N° 825575 and the Netherlands Organization for Scientific Research (Nederlandse Organisatie voor Wetenschappelijk Onderzoek) (NWO Veni 016.186.012). The 100,000 Genomes Project is managed by Genomics England Limited (a wholly owned company of the Department of Health and Social Care). The 100,000 Genomes Project is funded by the National Institute for Health Research and NHS England. The Wellcome Trust, Cancer Research UK, and the Medical Research Council have also funded research infrastructure of the 100,000 Genomes Project.

ACKNOWLEDGMENTS

The authors are grateful to the patients for their participation in this study. We thank Caro Bos, Larissa Govers, Edwin van Kaauwen, Dr. Bert van den Heuvel, Frans van den Brandt, and Gijs Franken for their excellent technical support. We thank Thijs Landman and Joeri van Strien for help with the conception of Seahorse_analyzeR. We thank Prof. dr. Robert Fenton for kindly providing the anti-pT58-NCC antibodies. This research includes data generated by the 100,000 Genomes Project. The 100,000 Genomes Project uses data provided by patients and collected by the National Health Service as part of their care and support.

Günter Klaus, Jean-Marie Coulibaly, Marion Vallet, Solenne Pelletier, Stéphane Decramer, Martin Kömhoff, Rolf Beetz, Mohan Shenoy, Karl P. Schlingmann, Detlef Bockenhauer, Rosa Vargas-Poussou, Pascal Houillier, Martin Konrad, Robert Kleta, André van Beek, Tom Nijenhuis, Andrew Mallett, and Chirag Patel were responsible for patient inclusion. Karl P. Schlingmann, Jeroen H.F. de Baaij, Detlef Bockenhauer, Melanie M.Y. Chan, Rosa Vargas-Poussou, Carsten Bergmann, Nine V.A.M. Knoers, André van Beek, Ernie M.H.F. Bongers, Albertien M. van Eerde, Tom Nijenhuis, Andrew Mallett, Marguerite Hureauux, Daan Viering, and Genomics England Research Consortium carried out the genetic investigations. Glenn Anderson and Eric J. Steenbergen performed histologic investigations. Daan Viering, Jeroen H.F. de Baaij, and Daan Panneman performed cell experiments. Karl P. Schlingmann, Jeroen H.F. de Baaij, Detlef Bockenhauer, Rosa Vargas-Poussou, René Bindels, Richard J. Rodenburg, Nine Knoers, Tom Nijenhuis, and Robert Kleta supervised the project. Jeroen H.F. de Baaij and Daan Viering drafted the manuscript. All authors were responsible for revision and approval of the manuscript.

Several authors of this publication are members of the European Reference Network for Rare Kidney Diseases (ERKNet)—Project ID No. 739532. Andrew Mallett was supported by an Royal Australasian College of Physicians Jacquot Research Establishment Fellowship and an Metro North Hospital and Health Service Clinical Research Fellowship.

SUPPLEMENTAL MATERIAL

This article contains the following supplemental material online at <http://jasn.asnjournals.org/lookup/suppl/doi:10.1681/ASN.2021050596/-/DCSupplemental>.

Supplemental Methods.

Supplemental Table 1. Primer and smMIP sequences.

Supplemental Table 2. Age-specific reference for urinary calcium/creatinine ratio.

Supplemental Table 3. Full clinical data.

Supplemental Table 4. Additional variant information.

Supplemental Table 5. Criteria for pathogenicity in each of the variants.

Supplemental Table 6. Number of phenylalanine and isoleucine residues in the mitochondrial genes.

Supplemental Figure 1. Thiazide test.

Supplemental Figure 2. Electron microscopy of proximal tubular cells.

Supplemental Figure 3. Control immunoblots $^{22}\text{Na}^+$ uptake experiments.

Supplemental Figure 4. Full immunoblot NCC phosphorylation experiments.

Supplemental Figure 5. NKCC2 phosphorylation with complex IV inhibition.

Supplemental Figure 6. Full immunoblot NKCC2 phosphorylation experiments.

REFERENCES

- Simon DB, Nelson-Williams C, Bia MJ, Ellison D, Karet FE, Molina AM, et al.: Gitelman's variant of Bartter's syndrome, inherited hypokalaemic alkalosis, is caused by mutations in the thiazide-sensitive Na-Cl cotransporter. *Nat Genet* 12: 24–30, 1996
- Blanchard A, Bockenhauer D, Bolignano D, Calò LA, Cosyns E, Devuyst O, et al.: Gitelman syndrome: consensus and guidance from a Kidney Disease: Improving Global Outcomes (KDIGO) Controversies Conference. *Kidney Int* 91: 24–33, 2017
- Vargas-Poussou R, Dahan K, Kahila D, Venisse A, Riveira-Munoz E, Debaix H, et al.: Spectrum of mutations in Gitelman syndrome. *J Am Soc Nephrol* 22: 693–703, 2011
- Downie ML, Lopez Garcia SC, Kleta R, Bockenhauer D: Inherited tubulopathies of the kidney: insights from genetics. *Clin J Am Soc Nephrol* 16: 620–630, 2020
- Viering DHM, de Baaij JHF, Walsh SB, Kleta R, Bockenhauer D: Genetic causes of hypomagnesemia, a clinical overview. *Pediatr Nephrol* 32: 1123–1135, 2017
- van der Made CI, Hoorn EJ, de la Faille R, Karaaslan H, Knoers NV, Hoenderop JG, et al.: Hypomagnesemia as first clinical manifestation of ADTKD-HNF1B: a case series and literature review. *Am J Nephrol* 42: 85–90, 2015
- Chinnery PF: Primary Mitochondrial disorders overview. In: GeneReviews®, edited by Adam MP AH, Pagon RA, et al.: Seattle, Washington, University of Washington, 2000
- Goto Y, Itami N, Kajii N, Tochimarum H, Endo M, Horai S: Renal tubular involvement mimicking Bartter syndrome in a patient with Kearns-Sayre syndrome. *J Pediatr* 116: 904–910, 1990
- Wilson FH, Hariri A, Farhi A, Zhao H, Petersen KF, Toka HR, et al.: A cluster of metabolic defects caused by mutation in a mitochondrial tRNA. *Science* 306: 1190–1194, 2004
- Giordano C, Powell H, Leopizzi M, De Curtis M, Travaglini C, Sebastiani M, et al.: Fatal congenital myopathy and gastrointestinal pseudo-obstruction due to POLG1 mutations. *Neurology* 72: 1103–1105, 2009
- Zhou Y, Zhong C, Yang Q, Zhang G, Yang H, Li Q, et al.: Novel SARS2 variants identified in a Chinese girl with HUPRA syndrome. *Mol Genet Genomic Med* 9: e1650, 2021
- Connor TM, Hoer S, Mallett A, Gale DP, Gomez-Duran A, Posse V, et al.: Mutations in mitochondrial DNA causing tubulointerstitial kidney disease. *PLoS Genet* 13: e1006620, 2017
- Li H, Durbin R: Fast and accurate long-read alignment with Burrows-Wheeler transform. *Bioinformatics* 26: 589–595, 2010
- Li H, Handsaker B, Wysoker A, Fennell T, Ruan J, Homer N, et al.; 1000 Genome Project Data Processing Subgroup: The Sequence Alignment/Map format and SAMtools. *Bioinformatics* 25: 2078–2079, 2009
- Martin AR, Williams E, Foulger RE, Leigh S, Daugherty LC, Niblock O, et al.: PanelApp crowdsources expert knowledge to establish consensus diagnostic gene panels. *Nat Genet* 51: 1560–1565, 2019
- Ekici AB, Hackenbeck T, Morinière V, Pannes A, Buettner M, Uebe S, et al.: Renal fibrosis is the common feature of autosomal dominant tubulointerstitial kidney diseases caused by mutations in mucin 1 or uromodulin. *Kidney Int* 86: 589–599, 2014
- Yarham JW, McFarland R, Taylor RW, Elson JL: A proposed consensus panel of organisms for determining evolutionary conservation of mt-tRNA point mutations. *Mitochondrion* 12: 533–538, 2012
- Wong LC, Chen T, Wang J, Tang S, Schmitt ES, Landsverk M, et al.: Interpretation of mitochondrial tRNA variants. *Genet Med* 22: 917–926, 2020
- Ellard S, Baple E, Callaway A, Berry I, Forrester N, Turnbull C, et al.: ACGS Best Practice Guidelines for Variant Classification in Rare Disease 2020, ACGS, 2020. Accessed March 1, 2021.
- Bech AP, Wetzels JFM, Nijenhuis T: Reference values of renal tubular function tests are dependent on age and kidney function. *Physiol Rep* 5: e13542, 2017
- Colussi G, Bettinelli A, Tedeschi S, De Ferrari ME, Syrén ML, Borsa N, et al.: A thiazide test for the diagnosis of renal tubular hypokalaemic disorders. *Clin J Am Soc Nephrol* 2: 454–460, 2007

22. Rodenburg RJT: Biochemical diagnosis of mitochondrial disorders. *J Inherit Metab Dis* 34: 283–292, 2011
23. Panneman DM, Wortmann SB, Haaxma CA, van Hasselt PM, Wolf NI, Hendriks Y, et al.: Variants in NGLY1 lead to intellectual disability, myoclonus epilepsy, sensorimotor axonal polyneuropathy and mitochondrial dysfunction. *Clin Genet* 97: 556–566, 2020
24. Yépez VA, Kremer LS, Iuso A, Gusic M, Kopajtic R, Koňáriková E, et al.: OCR-Stats: robust estimation and statistical testing of mitochondrial respiration activities using Seahorse XF Analyzer. *PLoS One* 13: e0199938, 2018
25. Pedersen NB, Hofmeister MV, Rosenbaek LL, Nielsen J, Fenton RA: Vasopressin induces phosphorylation of the thiazide-sensitive sodium chloride cotransporter in the distal convoluted tubule. *Kidney Int* 78: 160–169, 2010
26. Ashton EJ, Legrand A, Benoit V, Roncelin I, Venisse A, Zennaro MC, et al.: Simultaneous sequencing of 37 genes identified causative mutations in the majority of children with renal tubulopathies. *Kidney Int* 93: 961–967, 2018
27. World Health Organization: *Global Status Report on Noncommunicable Diseases 2014*, 2014. Available at: http://apps.who.int/iris/bitstream/handle/10665/148114/9789241564854_eng.pdf;jsessionid=51B6533AF532336F82399400471FA2AD?sequence=1. Accessed July 12, 2021.
28. World Health Organization: *Global Health Risks: Mortality and Burden of Disease Attributable to Selected Major Risks*, 2009. Available at: https://www.who.int/healthinfo/global_burden_disease/GlobalHealthRisks_report_full.pdf. Accessed July 12, 2021.
29. Walsh PR, Tse Y, Ashton E, Iancu D, Jenkins L, Bienias M, et al.: Clinical and diagnostic features of Bartter and Gitelman syndromes. *Clin Kidney J* 11: 302–309, 2018
30. Kidney Disease: Improving Global Outcomes: Autosomal dominant tubulointerstitial kidney disease: Diagnosis, classification, and management. https://kdigo.org/wp-content/uploads/2017/02/KDIGO_ADTKD-2015.pdf. Accessed March 15, 2021
31. Kunz WS, Kudin A, Vielhaber S, Elger CE, Attardi G, Villani G: Flux control of cytochrome c oxidase in human skeletal muscle. *J Biol Chem* 275: 27741–27745, 2000
32. Gnaiger E: Mitochondrial Pathways and Respiratory Control: An Introduction to OXPHOS Analysis. *Mitochondr Physiol Network* 19.12, Innsbruck, OROBOROS MiPNet Publications, 2014
33. Reilly RF, Ellison DH: Mammalian distal tubule: Physiology, pathophysiology, and molecular anatomy. *Physiol Rev* 80: 277–313, 2000
34. Belostotsky R, Ben-Shalom E, Rinat C, Becker-Cohen R, Feinstein S, Zeligson S, et al.: Mutations in the mitochondrial seryl-tRNA synthetase cause hyperuricemia, pulmonary hypertension, renal failure in infancy and alkalosis, HUPRA syndrome. *Am J Hum Genet* 88: 193–200, 2011
35. Hanna MG, Nelson IP, Morgan-Hughes JA, Wood NW: MELAS: A new disease associated mitochondrial DNA mutation and evidence for further genetic heterogeneity. *J Neurol Neurosurg Psychiatry* 65: 512–517, 1998
36. Goto Y, Nonaka I, Horai S: A mutation in the tRNA(Leu)(UUR) gene associated with the MELAS subgroup of mitochondrial encephalomyopathies. *Nature* 348: 651–653, 1990
37. Melone MA, Tessa A, Petrini S, Lus G, Sampaolo S, di Fede G, et al.: Revelation of a new mitochondrial DNA mutation (G12147A) in a MELAS/MERFF phenotype. *Arch Neurol* 61: 269–272, 2004
38. Giordano C, Perli E, Orlandi M, Pisano A, Tuppen HA, He L, et al.: Cardiomyopathies due to homoplasmic mitochondrial tRNA mutations: Morphologic and molecular features. *Hum Pathol* 44: 1262–1270, 2013
39. Cox R, Platt J, Chen LC, Tang S, Wong LJ, Enns GM: Leigh syndrome caused by a novel m.4296G>A mutation in mitochondrial tRNA isoleucine. *Mitochondrion* 12: 258–261, 2012
40. Gutiérrez Cortés N, Pertuiset C, Dumon E, Börlin M, Hebert-Chatelain E, Pierron D, et al.: Novel mitochondrial DNA mutations responsible for maternally inherited nonsyndromic hearing loss. *Hum Mutat* 33: 681–689, 2012
41. Schaller A, Desetty R, Hahn D, Jackson CB, Nuoffer JM, Gallati S, et al.: Impairment of mitochondrial tRNA^{Ala} processing by a novel mutation associated with chronic progressive external ophthalmoplegia. *Mitochondrion* 11: 488–496, 2011
42. Tzen C-Y, Tsai J-D, Wu T-Y, Chen B-F, Chen M-L, Lin S-P, et al.: Tubulointerstitial nephritis associated with a novel mitochondrial point mutation. *Kidney Int* 59: 846–854, 2001
43. D'Aco KE, Manno M, Clarke C, Ganesh J, Meyers KE, Sondheimer N: Mitochondrial tRNA(Phe) mutation as a cause of end-stage renal disease in childhood. *Pediatr Nephrol* 28: 515–519, 2013
44. Lorenz R, Ahting U, Betzler C, Heimering S, Borggrafe I, Lange-Sperandio B: Homoplasmy of the mitochondrial DNA mutation m.616T>C leads to mitochondrial tubulointerstitial kidney disease and encephalopathy. *Nephron* 144:156-160, 2020
45. Riedhammer KM, Braunisch MC, Günthner R, Wagner M, Hemmer C, Strom TM, et al.: Exome sequencing and identification of phenocopies in patients with clinically presumed hereditary nephropathies. *Am J Kidney Dis* 76: 460–470, 2020
46. Zhang C, Wang L, Zhang J, Su XT, Lin DH, Scholl UI, et al.: KCNJ10 determines the expression of the apical Na-Cl cotransporter (NCC) in the early distal convoluted tubule (DCT1). *Proc Natl Acad Sci U S A* 111: 11864–11869, 2014
47. Wang MX, Cuevas CA, Su XT, Wu P, Gao ZX, Lin DH, et al.: Potassium intake modulates the thiazide-sensitive sodium-chloride cotransporter (NCC) activity via the Kir4.1 potassium channel. *Kidney Int* 93: 893–902, 2018
48. Terker AS, Zhang C, McCormick JA, Lazelle RA, Zhang C, Meermier NP, et al.: Potassium modulates electrolyte balance and blood pressure through effects on distal cell voltage and chloride. *Cell Metab* 21: 39–50, 2015
49. Bockenauer D, Feather S, Stanescu HC, Bandulik S, Zdebek AA, Reichold M, et al.: Epilepsy, ataxia, sensorineural deafness, tubulopathy, and KCNJ10 mutations. *N Engl J Med* 360: 1960–1970, 2009
50. Konrad M, Vollmer M, Lemmink HH, VAN DEN Heuvel LPWJ, Jeck N, Vargas-Poussou R, et al.: Mutations in the chloride channel gene CLCNKB as a cause of classic Bartter syndrome. *J Am Soc Nephrol* 11: 1449–1459, 2000
51. Schlingmann KP, Renigunta A, Hoorn EJ, Forst AL, Renigunta V, Atanasov V, et al.: Defects in KCNJ16 cause a novel tubulopathy with hypokalemia, salt wasting, disturbed acid-base homeostasis, and sensorineural deafness. *J Am Soc Nephrol* 32: 1498–1512, 2021
52. Cuevas CA, Su X-T, Wang M-X, Terker AS, Lin D-H, McCormick JA, et al.: Potassium sensing by renal distal tubules requires Kir4.1. *J Am Soc Nephrol* 28: 1814–1825, 2017
53. Janssen AG, Scholl U, Domeyer C, Nothmann D, Leinenweber A, Fahlke C: Disease-causing dysfunctions of barttin in Bartter syndrome type IV. *J Am Soc Nephrol* 20: 145–153, 2009
54. Chen J-C, Lo Y-F, Lin Y-W, Lin S-H, Huang C-L, Cheng C-J: WNK4 kinase is a physiological intracellular chloride sensor. *Proc Natl Acad Sci U S A* 116: 4502–4507, 2019
55. Grimm PR, Coleman R, Delpire E, Welling PA: Constitutively active SPAK causes hyperkalemia by activating NCC and remodeling distal tubules. *J Am Soc Nephrol* 28: 2597–2606, 2017
56. Yang S-S, Fang Y-W, Tseng M-H, Chu P-Y, Yu IS, Wu H-C, et al.: Phosphorylation regulates NCC stability and transporter activity in vivo. *J Am Soc Nephrol* 24: 1587–1597, 2013
57. Hansell P, Welch WJ, Blantz RC, Palm F: Determinants of kidney oxygen consumption and their relationship to tissue oxygen tension in diabetes and hypertension. *Clin Exp Pharmacol Physiol* 40: 123–137, 2013
58. McCormick JA, Ellison DH: Distal convoluted tubule. *Compr Physiol* 5: 45–98, 2015
59. Hall AM, Rhodes GJ, Sandoval RM, Corridon PR, Molitoris BA: In vivo multiphoton imaging of mitochondrial structure and function during acute kidney injury. *Kidney Int* 83: 72–83, 2013

60. Bagnasco S, Good D, Balaban R, Burg M: Lactate production in isolated segments of the rat nephron. *Am J Physiol* 248: F522–F526, 1985
61. Meij IC, Koenderink JB, De Jong JC, De Pont JJ, Monnens LA, Van Den Heuvel LP, et al.: Dominant isolated renal magnesium loss is caused by misrouting of the Na⁺,K⁺-ATPase γ -subunit. *Ann N Y Acad Sci* 986: 437–443, 2003
62. Franken GAC, Adella A, Bindels RJM, de Baaij JHF: Mechanisms coupling sodium and magnesium reabsorption in the distal convoluted tubule of the kidney. *Acta Physiol (Oxf)* 231: e13528, 2021
63. Geven WB, Monnens LA, Willems HL, Buijs WC, ter Haar BG: Renal magnesium wasting in two families with autosomal dominant inheritance. *Kidney Int* 31: 1140–1144, 1987
64. Schlingmann KP, Bandulik S, Mammen C, Tarailo-Graovac M, Holm R, Baumann M, et al.: Germline de novo mutations in ATP1A1 cause renal hypomagnesemia, refractory seizures, and intellectual disability. *Am J Hum Genet* 103: 808–816, 2018
65. de Baaij JH, Dorresteyn EM, Hennekam EA, Kamsteeg EJ, Meijer R, Dahan K, et al.: Recurrent FXD2 p.Gly41Arg mutation in patients with isolated dominant hypomagnesaemia. *Nephrol Dial Transplant* 30: 952–957, 2015
66. Adalat S, Hayes WN, Bryant WA, Booth J, Woolf AS, Kleta R, et al.: HNF1B mutations are associated with a Gitelman-like tubulopathy that develops during childhood. *Kidney Int Rep* 4: 1304–1311, 2019
67. Kompatscher A, de Baaij JHF, Aboudehen K, Hoefnagels APWM, Igarashi P, Bindels RJM, et al.: Loss of transcriptional activation of the potassium channel Kir5.1 by HNF1 β drives autosomal dominant tubulointerstitial kidney disease. *Kidney Int* 92: 1145–1156, 2017
68. Ferrè S, Veenstra GJ, Bouwmeester R, Hoenderop JG, Bindels RJ: HNF-1B specifically regulates the transcription of the γ -subunit of the Na⁺/K⁺-ATPase. *Biochem Biophys Res Commun* 404: 284–290, 2011
69. Bech AP, Wetzels JF, Bongers EMHF, Nijenhuis T: Thiazide responsiveness testing in patients with renal magnesium wasting and correlation with genetic analysis: A diagnostic test study. *Am J Kidney Dis* 68: 168–170, 2016
70. Nozu K, Iijima K, Kanda K, Nakanishi K, Yoshikawa N, Satomura K, et al.: The pharmacological characteristics of molecular-based inherited salt-losing tubulopathies. *J Clin Endocrinol Metab* 95: E511–E518, 2010
71. Jeck N, Konrad M, Peters M, Weber S, Bonzel KE, Seyberth HW: Mutations in the chloride channel gene, CLCNKB, leading to a mixed Bartter-Gitelman phenotype. *Pediatr Res* 48: 754–758, 2000
72. Reilly RF, Huang CL: The mechanism of hypocalciuria with NaCl cotransporter inhibition. *Nat Rev Nephrol* 7: 669–674, 2011
73. Kovacicova J, Winter C, Loffing-Cueni D, Loffing J, Finberg KE, Lifton RP, et al.: The connecting tubule is the main site of the furosemide-induced urinary acidification by the vacuolar H⁺-ATPase. *Kidney Int* 70: 1706–1716, 2006
74. Roshan M, Kabekkodu SP, Vijaya PH, Manjunath K, Graw J: Analysis of mitochondrial DNA variations in Indian patients with congenital cataract. *Mol Vis* 18: 181–193, 2012
75. Elisaf M, Panteli K, Theodorou J, Siamopoulos KC: Fractional excretion of magnesium in normal subjects and in patients with hypomagnesemia. *Magnes Res* 10: 315–320, 1997

AFFILIATIONS

- ¹Department of Physiology, Radboud Institute for Molecular Life Sciences, Radboud University Medical Center, Nijmegen, The Netherlands
- ²Department of General Pediatrics, University Children's Hospital, Münster, Germany
- ³Reference Center for Hereditary Kidney and Childhood Diseases (Maladies rénales héréditaires de l'enfant et de l'adulte [MARHEA]), Paris, France
- ⁴Department of Genetics, Assistance Publique Hôpitaux de Paris, Hôpital Européen Georges-Pompidou, Paris, France
- ⁵Department of Nephrology, Radboud Institute for Molecular Life Sciences, Radboud University Medical Center, Nijmegen, The Netherlands
- ⁶Department of Renal Medicine, Townsville University Hospital, Townsville, Australia
- ⁷Queensland Conjoint Renal Genetics Service – Genetic Health Queensland, Royal Brisbane and Women's Hospital, Brisbane, Australia
- ⁸Department of Renal Medicine, University College London, London, United Kingdom
- ⁹Department of Endocrinology, University Medical Center Groningen, University of Groningen, Groningen, The Netherlands
- ¹⁰Genetics Department, University Medical Center Utrecht, Utrecht, The Netherlands
- ¹¹Service of Nephrology, Yves Le Foll Hospital, Saint Briec, France
- ¹²Department of Physiological Functional Investigations, Centre Hospitalier Universitaire de Toulouse, Université Paul Sabatier, Toulouse, France
- ¹³Pediatric Nephrology, Internal Medicine and Rheumatology, Southwest Renal Rare Diseases Centre (SORARE), University Children's Hospital, Toulouse, France
- ¹⁴Department of Nephrology, University Hospital–Lyon Sud, Lyon, France
- ¹⁵Kuratorium für Heimdialyse Pediatric Kidney Center, Marburg, Germany
- ¹⁶University Children's Hospital, Philipps-University, Marburg, Germany
- ¹⁷Johannes Gutenberg Universität Mainz, Zentrum für Kinder- und Jugendmedizin, Mainz, Germany
- ¹⁸Department of Paediatric Nephrology, Royal Manchester Children's Hospital, Manchester, United Kingdom
- ¹⁹Department of Pathology, Radboud University Medical Center, Nijmegen, The Netherlands
- ²⁰Department of Pathology, Great Ormond Street Hospital for Children National Health Service (NHS) Foundation Trust, London, United Kingdom
- ²¹Department of Human Genetics, Radboud University Medical Center, Nijmegen, The Netherlands
- ²²Limbach Genetics, Medizinische Genetik Mainz, Prof. Bergmann & Kollegen, Mainz, Germany
- ²³Department of Medicine, Division of Nephrology, University Hospital Freiburg, Germany
- ²⁴Radboud Center for Mitochondrial Medicine, Translational Metabolic Laboratory, Department of Pediatrics, Radboud University Medical Center, Nijmegen, The Netherlands
- ²⁵Department of Paediatric Nephrology, Great Ormond Street Hospital for Children NHS Foundation Trust, London, United Kingdom

²⁶Centre de Recherche des Cordeliers, Sorbonne Université, Institut National de la Santé et de Recherche Médicale (INSERM), Université de Paris, Centre National de la Recherche Scientifique (CNRS), Paris, France

²⁷Department of Physiology, Assistance Publique-Hôpitaux de Paris, Hôpital Européen Georges Pompidou, Paris, France

²⁸Department of Genetics, University Medical Center Groningen, University of Groningen, Groningen, The Netherlands

²⁹Renal Unit, Great Ormond Street Hospital for Children NHS Foundation Trust, London, United Kingdom

Gitelman-like syndrome caused by pathogenic variants in mtDNA
Viering et al.

Supplementary material

Table of contents

1. Supplementary Methods
2. Description of Supplementary Tables
 - a. Supplementary Table 1: primer and smMIP sequences
 - b. Supplementary Table 2: Age-specific reference for urinary calcium:creatinine ratio
 - c. Supplementary Table 3: Full Clinical data
 - d. Supplementary Table 4: Additional variant information
 - e. Supplementary Table 5: Criteria for pathogenicity in each of the variants
 - f. Supplementary Table 6: Number of phenylalanine and isoleucine residues in the mitochondrial genes
3. Supplementary Figure 1: Thiazide test
4. Supplementary Figure 2: Electron microscopy of proximal tubular cells
5. Supplementary Figure 3: Control immunoblots $^{22}\text{Na}^+$ uptake experiments
6. Supplementary Figure 4: Full immunoblot NCC phosphorylation experiments
7. Supplementary Figure 5: NKCC2 phosphorylation with complex IV inhibition
8. Supplementary Figure 6: Full immunoblot NKCC2 phosphorylation experiments

Supplementary methods

Determination of heteroplasmy

For determination of heteroplasmy levels, DNA was isolated from fibroblasts using the Qiagen QIAamp DNA mini kit (#51306) and/or whole blood by standard clinical procedures. Heteroplasmy percentage of the identified candidate variants was determined by analysis with single molecule Molecular Inversion Probes (smMIPs) in whole blood (for families 1, 2, 4, 6, 8) and in fibroblasts (for families 3, 4, 6, 11). In short, smMIPs were incubated with 200 ng gDNA for 16 hours for hybridization, extension and ligation. This was followed by exonuclease treatment, amplification, purification and sequencing on a NextSeq500 (Illumina) with a 2x150 bp paired-end run. Data-analysis was done with SeqNext (JSI). smMIP sequences are available in Supplementary Table 1. Read depth and variant percentage for individuals 5.II.6 and 6.II.2 is based on exome sequencing data. For family 10 and 12 this is based on long-read sequencing with the Sequel (Pacific Biosciences) and for individual 11.II.1 on the multi-gene panel results. Heteroplasmy measurements in family 13 were performed on DNA isolated from peripheral-blood leukocytes, saliva, urinary epithelial cells and fibroblasts, using labelled amplicons and tetra-primer amplification refractory mutation system PCR as described in (1). A variant was considered homoplasmic if coverage at the variant position was at least 300 and the percentage of reads with the variant was above 99%.

Statistical analysis of genetic data

Fisher's exact test to test the odds of observing a mtDNA variant 6 times (m.591C>T) or 3 times (m.4291T>C) in a cohort of 156 people while the population frequency was 1 in 304,823 or lower, was performed using R version 3.6.2 and the `fisher.test()` function. Corrected p-values were obtained by a Bonferroni correction for multiple testing, i.e., corrected p-values were calculated by multiplying the obtained p-value by 3 as we screened for three variants.

Fractional magnesium excretion

Fractional magnesium excretion (FEMg) was obtained at the same time as the serum magnesium measurements and was calculated with the following formula:

$$\text{FEMg} = (\text{magnesium}_{\text{urine}} * \text{creatinine}_{\text{serum}}) / (\text{creatinine}_{\text{urine}} * \text{magnesium}_{\text{serum}}) * 100.$$

Thiazide test

Thiazide tests were performed in two families in conformity with previously described protocols (2, 3). Subjects of family 4 and 12 were allowed a small breakfast without coffee on the morning of the test, and a maximum of two sandwiches during the test. Baseline measurements (weight, blood pressure and first urine sample) were taken at 8 AM ($t = 0$). Subjects were then instructed to drink 10 mL/kg body weight in 15 minutes. A urine sample was again collected at $t = 45$ minutes, $t = 90$ and $t = 120$. At $t = 150$, blood and urine samples were collected and 50 mg of hydrochlorothiazide was given orally. During this last phase, subjects were instructed to drink 250 mL water per hour until the end of the test. Urine was

collected every 30-60 minutes until $t = 510$. An additional blood sample was collected at $t = 270$ and $t = 510$. At $t = 510$ body weight and blood pressure were measured again, as well as serum electrolytes, before safely ending the test.

A similar protocol was used for the thiazide test in the proband of family 1. This patient was asked to fast from midnight until 11 AM. The subject voided all urine at 7 AM ($t = 0$) and she was instructed to drink 450 mL of water. At $t = 60$ minutes, 50 mg hydrochlorothiazide was given orally. Blood samples were collected at $t = 60$ (baseline) and $t = 180$, while urine samples were collected at $t = 60$ (baseline), $t = 120$, $t = 180$ and $t = 240$. From $t = 60$ until $t = 240$, the patient was asked to drink 200 mL per hour.

Calculation of the fractional chloride excretion (FeCl) was done using the formula $(Cl_{urine} * creatinine_{serum}) / (creatinine_{urine} * Cl_{serum}) * 100$. For determining the maximal change in FeCl, we subtracted the average of the FeCl at baseline from the highest FeCl measurement obtained in the six hours after the administration of hydrochlorothiazide.

Values obtained with the thiazide test were compared to reference values determined by Colussi et al.(3) and that have been used before in our center.(2, 4) Colussi et al.(3) reported a diagnostic sensitivity 93% and specificity of 100% for Gitelman syndrome. Later, it was shown to have a lower specificity when it is used to discriminate Gitelman syndrome from Gitelman-like syndromes.(4) Test sensitivity in Gitelman-like syndromes is currently difficult to assess due to the small number of patients and conflicting results,(3-5) but seems to be significantly lower than for Gitelman syndrome.

Fibroblasts

In families 3 and 4, fibroblasts were grown from a skin biopsy. In families 6 and 11, fibroblasts were obtained by nasal brush (Cytobrush Plus, Cooper Surgical, # 176291). After initial culturing of the material at local laboratories, further experiments were performed at the Radboudumc, Nijmegen. Fibroblasts were cultured in Medium 199 (M199) (#P04-07050, Pan Biotech) supplemented with 10% (v/v) fetal calf serum (#10270, Gibco), 100 IU/mL penicillin and 100 µg/mL streptomycin (#15140-122, Gibco) in a humidified atmosphere with 5% (v/v) CO₂ at 37°C. For starting up cultures, 20% (v/v) fetal calf serum was used instead of 10%. All cultures were mycoplasma negative. For all experiments, fibroblasts with passage number between 5 and 20 were used. In addition to one family control (unaffected relative on the paternal line, control 1), two control cell lines of unrelated individuals were included. Both had been shown to have normal mitochondrial function in earlier experiments. One fibroblast line was derived from a skin biopsy done at the Radboudumc, Nijmegen (control 2), the other was obtained commercially (ATCC® PCS-201-012™, lot # 61683453, from a 40-year-old woman, control 3). Cell lines were tested for mycoplasma contamination after arrival and upon defrosting.

OXPPOS activity measurement

Measurements of the activity of the mitochondrial oxidative phosphorylation (OXPPOS) complexes were performed in a clinically certified setting as described previously (6). In short,

mitochondria were isolated from ~10 million cells by mechanical pottering and differential centrifugation. OXPHOS activity of each of the five mitochondrial complexes was determined by the rate of rotenone-sensitive DCIP reduction (complex I), malonate-sensitive DCIP reduction (complex II), cytochrome c reduction (complex III), cytochrome c oxidation (complex IV) and oligomycin-sensitive NADH oxidation (complex V). Additionally, citrate synthase activity and protein concentration were measured. Citrate synthase activity was measured by a colorimetric method (formation of 5-thio-2-nitrobenzoic acid, TNB, from di-5-thio-2-nitrobenzoic acid, DTNB, when acetyl-CoA and oxaloacetate are converted to citrate), protein concentration was measured by the absorption at 600 nm after adding pyrogallol red-molybdate. Obtained values were compared to reference values specific for our center.

Mitochondrial respiration by the Seahorse XFe96 Analyzer

Fibroblasts were trypsinized and counted on a Luna-II automatic cell counter (Logos biosystems, with cell counting slides #L12003). 1.5×10^4 cells were seeded per well (top and bottom rows were not used), and kept at 37°C, 5% (v/v) CO₂ for 20-24 hours. The Seahorse sensor cartridge was incubated overnight in calibrant buffer (Agilent, #102416-100). Seahorse XF base medium (Agilent #103334-100) was supplemented with L-glutamine (final concentration 2 mM, Life sciences), glucose (10 mM, Sigma) and pyruvate (1 mM, Gibco). Medium pH was set to 7.40 with NaOH (and if needed HCl) at 37°C and filtered (0.2 µm filter). 180 µL of warm medium was added to each well, including top and bottom rows. Plates were then incubated at 37°C, 0% CO₂ for 1-1,5 hour. After sensor calibration, cell plates were inserted in the Seahorse XFe96 analyzer and 16 measurements of OCR and ECAR (extracellular acidification rate) were done with 6-minute intervals: 3 minutes mixing and 3 minutes measuring. Directly after measurement 4 we injected oligomycin A (1 µmol/L final concentration, Sigma), after measurement 7 we injected 3 or 5 µmol/L FCCP (carbonyl cyanide 4-(trifluoromethoxy)phenylhydrazone, Sigma), after measurement 10 again FCCP (+1 µmol/L to obtain 4 and 6 µmol/L as final concentrations) and after measurement 13 rotenone 0.5 µmol/L (Sigma) and antimycin A 0.5 µmol/L (Sigma). To reduce inter-plate variation and differences between cell lines, within-plate titration was performed to identify the FCCP concentration at which respiration was maximally uncoupled.

Citrate synthase activity measurements for Seahorse XFe96 experiments

A modified version of the previously described protocol (7) was applied using DTNB (5,5'-dithiobis-2-nitrobenzoic acid; Sigma, #D8130). Seahorse medium was replaced by 20 µL of 0.33% (v/v) Triton X-100 (GE, #17-1315-01) in 10 mM Tris-HCl (pH 7.6), after which plates were stored at -80°C. Plates were subjected to in total 3 freeze-thaw cycles to interrupt all lipid bilayers. 150 µL with 0.17 mM DTNB, 0.035% Triton X-100 solution and 20 µL of 3 mM acetyl-CoA (#10101907001, Sigma) was added to each well. A Tecan Spark spectrophotometer (Tecan, Switzerland) measured background DTNB conversion for 9 minutes at 1-minute intervals (412 nm and 37°C). Subsequently, 10 µL of 10 mmol/L oxaloacetate (Sigma, #O4126) was added to each sample to start the reaction, and the same

measurement cycle was repeated immediately (412 nm and 37°C). Citrate synthase activity was calculated with the following formula:

$$\text{Citrate synthase activity} = (\text{DTNB}_{\text{conversion in presence of oxaloacetate}} - \text{DTNB}_{\text{background conversion}}) / (13.6 * 0.63) * (1/5)$$

The 13.6 indicates an extinction coefficient of 13.6/mmol/L/cm, the 0.63 the distance that the light travels through the solution in cm and the 1/5 that the reaction volume is 1/5th of 1 mL (200 µL). The result is expressed in mU/mL and represents the citrate synthase activity of 1 confluent Seahorse XFe96 well dissolved in 1 mL.

Seahorse AnalyzeR

In short, a text file containing the normalized and background-subtracted OCR values was exported from Wave Desktop Software and analyzed in R, version 3.6.2 for Mac, using Rstudio version 1.1.456. The R-script depends on packages data.table (version 1.12.8) and tidyverse (1.3.0). OCR values < 0 were removed. For each well, the median OCR of each Mito Stress test interval was calculated. Subsequently, for each cell line, the average of all wells on one plate was calculated ($n = 6-12$). For interval 3, the concentration of the uncoupling agent FCCP (carbonyl cyanide 4-(trifluoromethoxy)phenylhydrazone, Sigma) resulting in the highest average OCR was selected. Then, all wells that did not respond correctly to the Mito Stress test were removed (i.e., not *interval 3 > interval 1 > interval 2 > interval 4*). Maximum respiration was obtained by subtracting the average OCR of interval 4 from the average OCR of interval 3. Lastly, by expressing the data as a percentage from the average of the three control cell lines on the plate, the effect of the inter-plate effect was reduced.

Preparation of buffers for ²²Na⁺ uptake and NCC phosphorylation experiments

Hypotonic-low-chloride buffer was prepared as 70 mmol/L sodium gluconate, 0.5 mmol/L calcium gluconate, 0.5 mmol/L magnesium chloride, 2.5 mmol/L potassium gluconate, 2.5 mmol/L HEPES (i.e., 4-(2-hydroxyethyl)-1-piperazineethanesulfonic acid) and set to pH 7.4 with Tris. Isotonic buffer was prepared as 140 mmol/L sodium chloride, 1 mmol/L calcium chloride, 1 mmol/L magnesium chloride, 5 mmol/L potassium chloride, 5 mmol/L HEPES and also set to pH 7.4 with Tris. Lysis buffer contained the following: 1 mmol/L EGTA (ethylene glycol-bis(β-aminoethyl ether)-N,N,N',N'-tetraacetic acid), 1 mmol/L EDTA (Ethylenediaminetetraacetic acid), 10 mmol/L sodium glycerophosphate, 50 mmol/L sodium fluoride, 10 mmol/L sodium pyrophosphate, 270 mmol/L sucrose, 150 mmol/L sodium chloride, 1 mmol/L sodium orthovanadate and 50 mmol/L Tris, set to pH 7.5 with hydrochloric acid. 1% (v/v) Triton X-100 and protease inhibitors (pepstatin 1 µg/mL, leupeptin 5 µg/mL, aprotinin 1 µg/mL and PMSF (phenylmethylsulphonyl fluoride) 1 mmol/L) were added fresh.

Effect of complex IV inhibition on NCC-mediated ²²Na⁺ uptake

HEK293 cells with passage number 10-20 were seeded on 24-well plates (#734-1604, Costar) coated with poly-L-lysine (#P2636, Sigma), at a density of 8×10^4 cells per well. We transfected each well with either 0.5 µg DNA construct containing NCC (pCIneo-NCC-IRES-GFP) or 0.5 µg

construct without NCC (pCIneo-IRES-GFP, hereafter indicated with mock). Transfection was done within 24 hours using lipofectamine (#11668019, Invitrogen; DNA:lipofectamine ratio 1:2) according to the manufacturer's protocol, including supplementation with opti-MEM (#31985-054, Gibco). After two days, transfection success was assessed by visually checking GFP expression under the microscope. Samples were subsequently put on hypotonic-low-chloride or isotonic buffer with or without 100 $\mu\text{mol/L}$ thiazide, and with either 1 mmol/L potassium cyanide (KCN, experimental condition) or as a control 1 mmol/L potassium chloride (KCl). After half an hour incubation, samples were put on isotonic buffer containing both $^{22}\text{Na}^+$ and inhibitors of other sodium transporters and channels (i.e., amiloride 100 $\mu\text{mol/L}$, bumetanide 100 $\mu\text{mol/L}$ and ouabain 1 mmol/L). After half an hour in the $^{22}\text{Na}^+$, cells were lysed in 500 μL of 0.1% (w/v) SDS (sodium dodecyl sulfate) in PBS (phosphate buffered saline). 3.5 mL of Opti-Fluor (#6013199, Perkin Elmer) was added and after thorough mixing, radioactivity was measured on a liquid scintillation counter (Hidex 600SL). Radioactive buffers were also measured on the counter to exclude differences in $^{22}\text{Na}^+$ concentration between the different buffers. Samples were counted for 180 seconds with a coincidence time of 35 nanoseconds. Wavelength measurement window was set at 300-700nm. Ionizer delay was set to 10 seconds, measurement chamber delay to 5 seconds. NCC expression was assessed by immunoblotting, following the same protocol as described below. Culturing and the $^{22}\text{Na}^+$ uptake was done in triplicate, the complete experiment was performed four times.

NCC phosphorylation experiments

Culturing and transfection was done the same as for the $^{22}\text{Na}^+$ uptake experiments, with the following changes. Cells were seeded in 6-well plates at a density of 4×10^5 cells per well. Transfection was performed with 2 μg NCC or mock construct. Two days after transfection, samples were put on hypotonic-low-chloride or isotonic buffer with or without 100 $\mu\text{mol/L}$ thiazide, and with either 1 mmol/L potassium cyanide (KCN, experimental condition) or as a control 1 mmol/L potassium chloride (KCl). Cells were lysed in 200 μL ice-cold lysis buffer. Culturing was done in duplicate; the complete experiment was performed three times.

NKCC2 phosphorylation experiments

HEK293 cells with passage number 10-14 were seeded on 10cm petri-dishes (Cellstar, #664160) coated with poly-L-lysine (#P2636, Sigma), at a density of 4×10^6 cells per dish. We transfected each well with either 14 μg DNA construct containing human NKCC2 isoform A (pCIneo-NKCC2-HA-IRES-GFP) or 14 μg construct without NKCC2 (pCIneo-IRES-GFP, hereafter indicated with mock). Transfection was done within 24 hours at 50-80% confluency using lipofectamine (#11668019, Invitrogen; DNA:lipofectamine ratio 1:2) according to the manufacturer's protocol, including supplementation with opti-MEM (#31985-054, Gibco). Samples were subsequently put on hypotonic-low-chloride or isotonic buffer with either 1 mmol/L potassium cyanide (KCN, experimental condition) or as a control 1 mmol/L potassium chloride (KCl) for 30 minutes. Cells were lysed in 1 mL ice-cold lysis buffer. Culturing was done in duplicate; the complete experiment was performed three times.

Measuring protein concentration

Protein concentration was measured by adding 200 μ L of Bradford reagent (Sigma-Aldrich, #B6916-500ML) to 5 μ L of diluted sample, measuring light absorbance at 595 nm with a Benchmark Plus microplate reader (Bio-Rad), and calculating protein concentration by comparing the absorbance to a standard curve of known protein concentrations (diluted albumin standard, ThermoFisher Scientific, #23209).

Immunoprecipitation (NKCC2 only)

Pierce anti-HA beads (Thermo Scientific, #26181) were washed 4 times with PBS, spinning the beads down at 1,600 rpm in between washes. 4.5 mg of the protein sample was added to 40 μ L of 1:1 beads:PBS solution and incubated on a rotor overnight. Beads were washed 3 times with ice-cold lysis buffer, supernatant was removed and the beads were incubated with 30 μ L 2x Laemmli-dithiothreitol (DTT) buffer for 30 minutes at 37°C. The supernatant was subsequently used for SDS-PAGE immunoblotting.

Immunoblotting NCC

Equal amounts of protein were supplemented with Laemmli buffer (final concentration 1x) and dithiothreitol (final concentration 100 mmol/L). 25 μ g of protein of each sample was subjected to SDS-PAGE (8% 40:1 bisacrylamide gel) and transferred to polyvinylidene membranes by blotting at 100 volts for 2 hours on ice. Membranes underwent blocking in 5% (w/v) non-fat dry milk dissolved in 1x Tris-buffered saline with 0.1% Tween-20 (TBS-T) for 60 minutes at room temperature. Incubation of the membranes with primary antibody was done overnight at 4°C: rabbit anti-NCC (1:2000, Millipore, #AB3553), rabbit anti-pT58-NCC (NCC phosphorylated at human position p.Thr60, 1:2000, kind gift from Robert Fenton(8)). Specificity of antibodies was confirmed by the inclusion of a negative control in all experiments (i.e., HEK293 cells transfected with a mock construct instead of NCC construct, Supplementary Figure 3). Membranes were subsequently washed three times with TBS-T and incubated in secondary antibody for 1 hour at room temperature (peroxidase anti-rabbit-IgG, 1:10 000, Sigma Aldrich, #A4914). Three more washes with TBS-T were performed, after which proteins were visualized with chemiluminescent reagent (SuperSignal West femto/pico, Thermo Fisher Scientific, # 34095/#34078) on an ImageQuant LAS 4000 (Supplementary Figure 2). Densitometric analysis of band intensities was done using ImageJ Software (version 1.51).

Immunoblotting NKCC2

1 μ L of PNGase F (NEB, P0704) was added to the Laemmli-DTT samples and incubated for 30 more minutes at 37°C. 10 μ L of sample was subjected to SDS-PAGE (7% 40:1 bisacrylamide gel). Transfer to a membrane and blocking was performed the same as for NCC. Incubation of the membranes with primary antibody was done overnight at 4°C: sheep anti-NKCC2 (1 μ g/mL, bought from MRC Dundee (contact: James Hastie), sheep anti-pS91-NKCC2 (NKCC2

phosphorylated at human position p.Ser91, 1 µg/mL + 10 µg/mL non-phospho-peptide, bought from MRC Dundee (contact: James Hastie). Specificity of antibodies was confirmed by the inclusion of a negative control in all experiments (i.e., HEK293 cells transfected with a mock construct). Membranes were subsequently washed three times with TBS-T and incubated in secondary antibody for 1 hour at room temperature (peroxidase anti-sheep-IgG, 1:10 000, Jackson ImmunoResearch, #213-032-177). Subsequent washing and imaging was the same as for NCC.

Software and websites used for genetic analyses

- OMIM: <https://omim.org/>. Identifiers of syndromes named in the text: Gitelman syndrome/biallelic pathogenic variants in *SLC12A3* (263800), biallelic pathogenic variants in *CLCNKB* (607364), monoallelic pathogenic variant in *HNF1B* (137920), monoallelic pathogenic variant in *FXYD2* (154020), biallelic pathogenic variant in *KCNJ10* (612780), monoallelic pathogenic variant in *ATP1A1* (618314), biallelic pathogenic variants in *EGF* (611718), HUPRA syndrome (613845), Kearns-Sayre syndrome (530000), congenital myopathy and gastro-intestinal pseudo-obstruction (613662), hypercholesterolemia with hypertension (500005), MELAS (540000), MT-TI associated cardiomyopathy (*590045), Leigh syndrome (256000), nonsyndromic hearing loss (500008).
- MITOMAP: A Human Mitochondrial Genome Database. <http://www.mitomap.org>, 2021. A database of mitochondrial variation based on GenBank. Accessed on June 28, 2021. The database at that moment contained 51 836 full sequences from GenBank. As a caveat, sequences from GenBank might not be of equal quality and are considered enriched for patients with mitochondrial disease.
- HelixMTdb: <https://www.helix.com/pages/research>. A population-based database of mitochondrial variation -accessed on June 28, 2021- contained sequences from 196,554 unrelated individuals.
- Gnomad: <https://gnomad.broadinstitute.org/>. Accessed June 28, 2021, version 3.1.1. A population-based database of mitochondrial variation -accessed on June 28, 2021- contained sequences from 56,434 unrelated individuals.
- MitoTIP: accessible via https://www.mitomap.org/mitomaster/index_snvs.cgi, accessed on June 28, 2021. Predicts pathogenicity of mitochondrial tRNA variants based on variant frequency in GenBank, annotations of pathogenicity from MITOMAP, conservation across species, the position of the variant within the tRNA and the type of nucleotide change (transition/transversion).
- PON-mt-tRNA: <http://structure.bmc.lu.se/PON-mt-tRNA/>. Accessed on June 28, 2021. Machine-learning based predictor of pathogenicity of mitochondrial tRNA variants. This algorithm is not influenced as much by GenBank records or literature reports on the variant.
- Clustal O: <https://www.ebi.ac.uk/Tools/msa/clustalo/> for aligning the sequence of *MT-TI* and *MT-TF* of the 10 selected species. Default settings were used, and small manual alterations were done to improve alignment. Used accession numbers of the mitochondrial genome, from Homo sapiens to Drosophila melanogaster in the same

order as figure 2: NC_012920.1, NC_001643, NC_001644, NC_002082, NC_005089, NC_001665.2, NC_006853.1, NC_040970.1, NC_002081, NC_024511.2.

- rtools: <http://rtools.cbrc.jp/cgi-bin/index.cgi> for modelling of tRNA secondary structure with CentroidHomFold. Default settings were used (inference engines: *McCaskill(BL)* and *CONTRAlign*, base pair weight: 2^3 , E-value for homology search against Rfam: *0.01*, number of homologous sequences: *30*). Accessed 5 September 2020.
- R version 3.6.2 for Mac, using Rstudio version 1.1.456.
 - The code written for analysis of Seahorse XFe96 data has been made publicly: <https://github.com/DaanViering/Seahorse-analyzeR>. Version 1.2 of date 26-03-2021 was used.
 - Code for Fisher's exact test:

```
> x <- data.frame(c(6,156), c(1,304824))
> fisher.test(x)
```
- Mthap: For mitochondrial haplogroup determination. <https://dna.jameslick.com/mthap/>
- ClinVar: <https://www.ncbi.nlm.nih.gov/clinvar/>. Variant classifications were submitted to ClinVar in July 2021, accession numbers: SCV001745859, SCV001739513, SCV001745860, SCV001745835

Supplementary table 1: primer and smMIP sequences

Nucleotide sequences of the primers and single molecule Molecular Inversion probes (smMIPs) used. Start and end indicate positions in the mitochondrial genome.

Primer/smMIP	Sequence	Start	End
MT-TF sequencing primer forward	ACCCTAACACCAGCCTAACCA	368	388
MT-TF sequencing primer reverse	GCTTGTTCCTTTTGATCGTGGTG	734	756
MT-TI sequencing primer forward	GTCACCAAGACCCTACTTCTAACC	4084	4107
MT-TI sequencing primer reverse	GCTGTGATGAGTGTGCCTGC	4512	4531
MT-TF smMIP 1	GGTTTGGTCCTAGCCTTTCNNNNNNNNCTTCAGC TTCCCGATATCCGACGGTAGTGTACACCGCTGCTA ACCCCATAC	542	651
MT-TF smMIP 2	AGGATGGGCGGGGGTGTATTGNNNNNNNNCT TCAGCTTCCCGATATCCGACGGTAGTGTGATGTG AGCCCGTCTAAA	508	617
MT-TF smMIP 3	AAGCTACATAAACTGTGGNNNNNNNNCTTCAGC TTCCCGATATCCGACGGTAGTGTAACTCACTGGA ACGGGGATGCT	590	699
MT-TI smMIP 1	AATCCAAAATTCTCCGTGCCNNNNNNNNCTTCAG CTTCCCGATATCCGACGGTAGTGTATTACAATCTC CAGCATTCC	4251	4360
MT-TI smMIP 2	GGTAGGAAGTTTTTTCATAGGANNNNNNNNCTT CAGCTTCCCGATATCCGACGGTAGTGTGTTTAAG CTCCTATTATT	4191	4300
MT-TI smMIP 3	CATATTTCTTAGGTTTGANNNNNNNNCTTCAGCT TCCCGATATCCGACGGTAGTGTCTTTAGGATGGG GTGTGATAGG	4272	4381

Supplementary Table 2: Age-specific reference for urinary calcium:creatinine ratio
Age-specific reference for urinary calcium:creatinine ratio. m, month; y, year.

Age group	Normal calcium/creatinine ratio (mmol/mmol)
1 m - 1 y	0.09 - 2.2
1 - 2 y	0.07 - 1.5
2 - 3 y	0.06 - 1.4
3 - 5 y	0.05 - 1.1
5 - 7 y	0.04 - 0.8
7 - 17 y	0.04 - 0.7
Adults	0.16-0.7

Supplementary Table 3: Full clinical data

All available relevant clinical data on patients included in this study. CKD, chronic kidney disease as defined by KDIGO; eGFR, estimated glomerular filtration rate; RBP, retinol-binding protein. Please find this table as a supplementary Excel attachment.

Supplementary Table 4: Additional variant information

Variant information obtained from different databases. For PON-mt-tRNA the cut-off for likely pathogenic is > 0.5, for MITOTIP, the cut-off is > 12.66. Higher scores denote a higher probability of pathogenicity. The sensitivity and specificity of MITOTIP are slightly higher than those of PON-mt-tRNA. The numbers written in brackets in the column headers represent the number of individuals included in each population database. Position indicates position of the variant on the mitochondrial genome. Ref, reference allele; Alt, alternative allele; VUS, variant of uncertain significance.

Position	Ref	Alt	Gene	HelixMTdb (196,554)	gnomAD (56,434)	GenBank Seqs (MITOMAP) (51,836)	MITOTIP	PON-mt-tRNA
591	C	T	MT-TF	Homoplasmic: 0 Heteroplasmic: 3	Homoplasmic: 0 Heteroplasmic: 1	0	3.2	0.11
616	T	C	MT-TF	Homoplasmic: 0 Heteroplasmic: 6	0	1	17.5	0.18
4291	T	C	MT-TI	0	0	0	10.0	0.34
643	A	G	MT-TF	Homoplasmic: 3 Heteroplasmic:1	0	0	11.27	0.59

Supplementary Table 5: Criteria for pathogenicity in each of the variants

Criteria are applied as proposed by Wong et al.(9) Position indicates position of the variant on the mitochondrial genome. References in this table.(1, 9-12) Ref, reference allele; Alt, alternative allele; VUS, variant of uncertain significance.

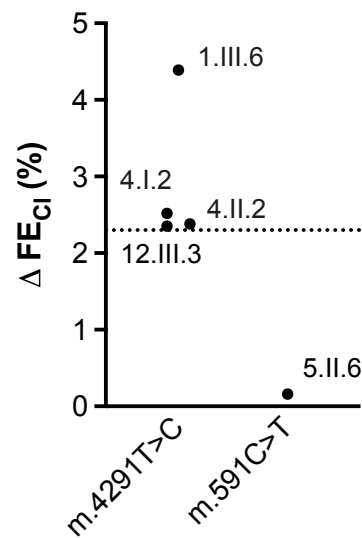
Position	Ref	Alt	Gene	Criteria for pathogenicity added based on this study	Criteria for pathogenicity previously met	References	Verdict
591	C	T	MT-TF	PS4, PM9, PM10, PP6, PP7, BP4	N.A.	None	Pathogenic
616	T	C	MT-TF	-	PS5, PM7, PM9, PM10	Connor et al. 2017, Wong et al. 2020, Riedhammer et al. 2020, Lorenz et al. 2020	Pathogenic
4291	T	C	MT-TI	PS4, PM9, PM10, PP6	PP7, PS5	Wilson et al. 2004, Roshan et al. 2012	Pathogenic
643	A	G	MT-TF	PM9, PM10	BS4, PP7	Wong et al. 2020	VUS

Supplementary Table 6: Number of phenylalanine and isoleucine residues in the mitochondrial genes

Number of phenylalanine and isoleucine residues in the mitochondrial genes, and their relative abundance in all mitochondrial genes.

Gene	Subunit	# of phenylalanine residues	# of isoleucine residues	# total residues	Ratio phenylalanine residues/total residues (%)	Ratio isoleucine residues/total residues (%)
ND1	I	16	22	318	5.0	6.9
ND2	I	15	31	347	4.3	8.9
ND3	I	8	9	115	7.0	7.8
ND4	I	20	41	459	4.4	8.9
ND4L	I	3	7	98	3.1	7.1
ND5	I	38	54	603	6.3	9.0
ND6	I	8	12	174	4.6	6.9
CYB	III	24	38	380	6.3	10.0
COX1	IV	41	38	513	8.0	7.4
COX2	IV	10	22	227	4.4	9.7
COX3	IV	23	14	261	8.8	5.4
ATP6	V	9	29	229	3.9	12.7
ATP8	V	1	3	68	1.5	4.4

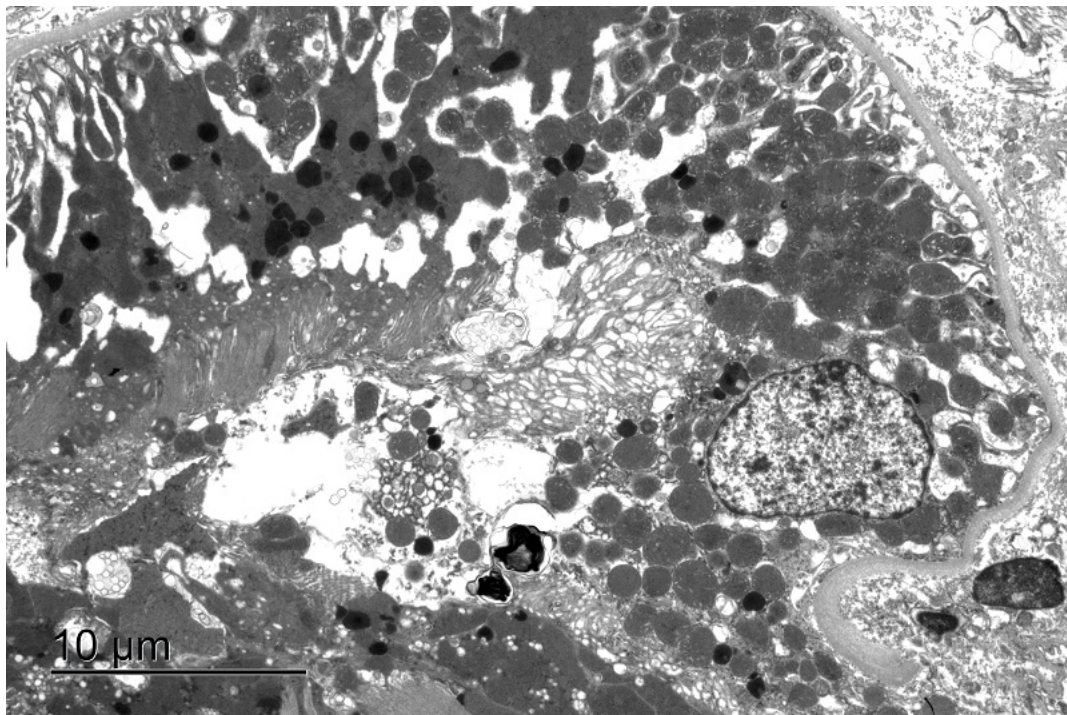
Supplementary Figure 1: Thiazide test



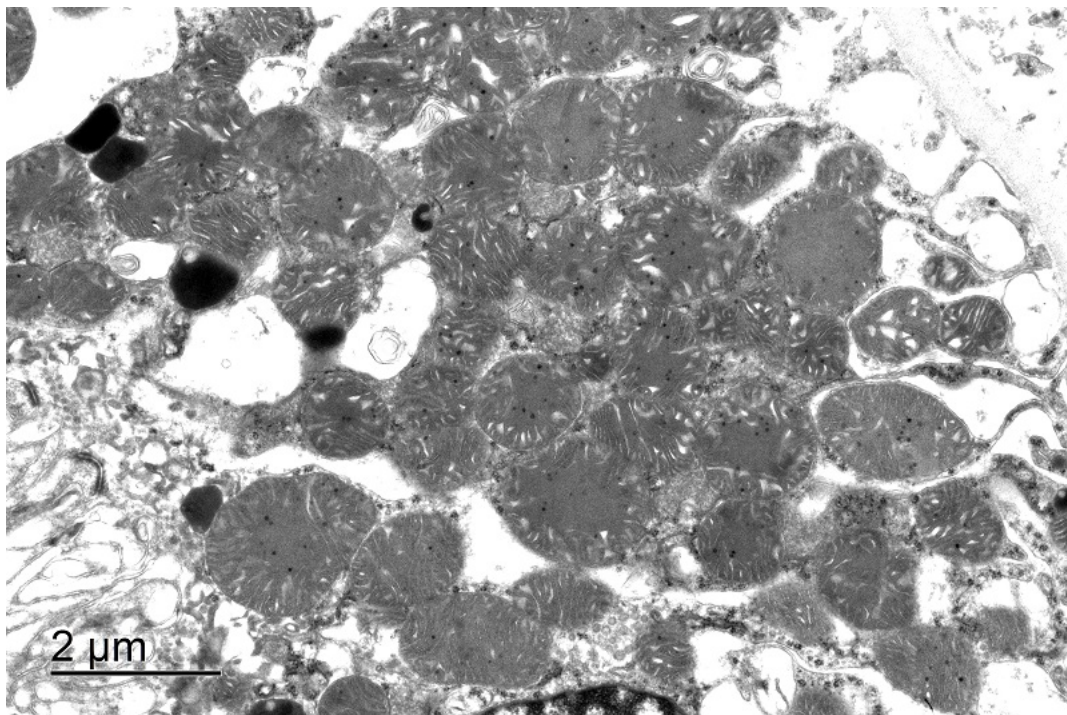
Maximal change in the fractional excretion of chloride (ΔFE_{Cl}) after administration of a single dose of 50 mg hydrochlorothiazide orally. The followed protocols were slightly different per patient as described in the Supplementary Methods. The dotted line represents the cut-off value proposed by Colussi et al. (3) for Gitelman syndrome. Patients with Gitelman syndrome typically have a ΔFE_{Cl} values below this cut-off, i.e., below 2.3%.

Supplementary Figure 2: Electron microscopy of proximal tubular cells

A

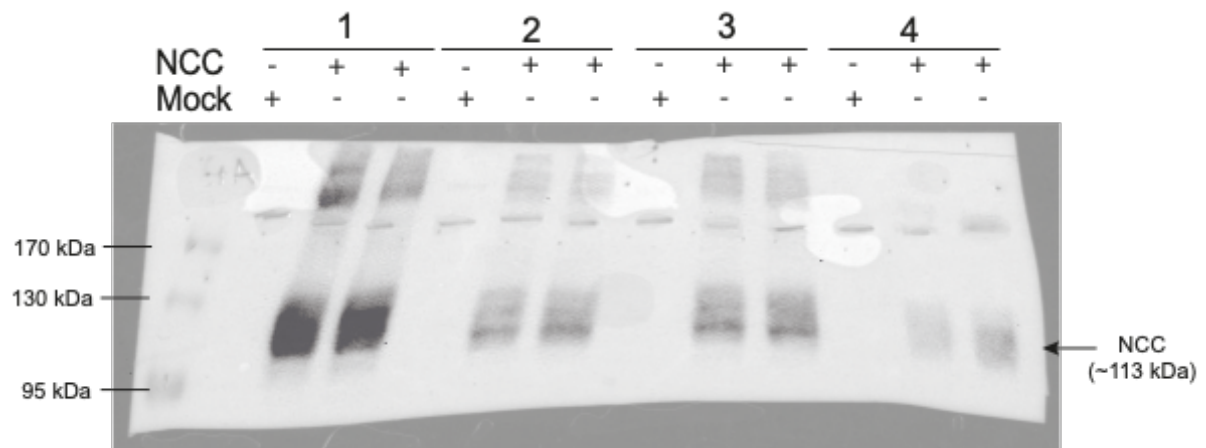


B



Examination of proximal tubular cells in the kidney biopsy of patient 10.II.3. (A) Note the apical brush border that is specific for the proximal tubule. Mitochondria look enlarged and abnormal in shape. (B) A close-up of part of panel A shows that most mitochondria exhibit widened cristae structures and sometimes partial absence of cristae. This contrasts with the distal tubular cells shown in Figure 4 D-E; there, cristae were not visible at all in most mitochondria.

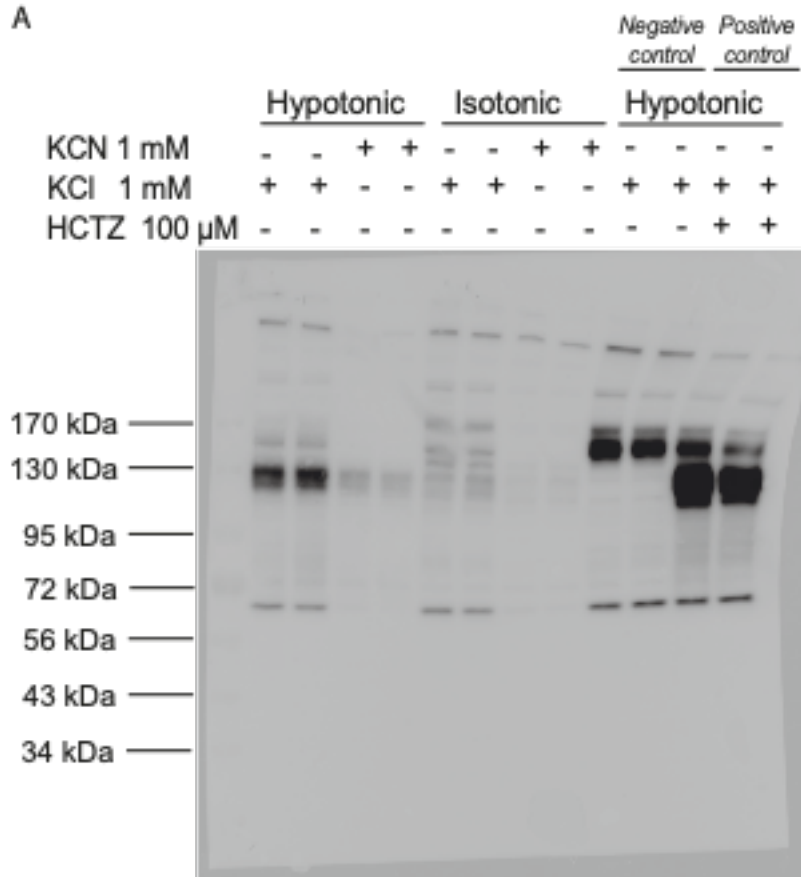
Supplementary Figure 3: Control immunoblots $^{22}\text{Na}^+$ uptake experiments



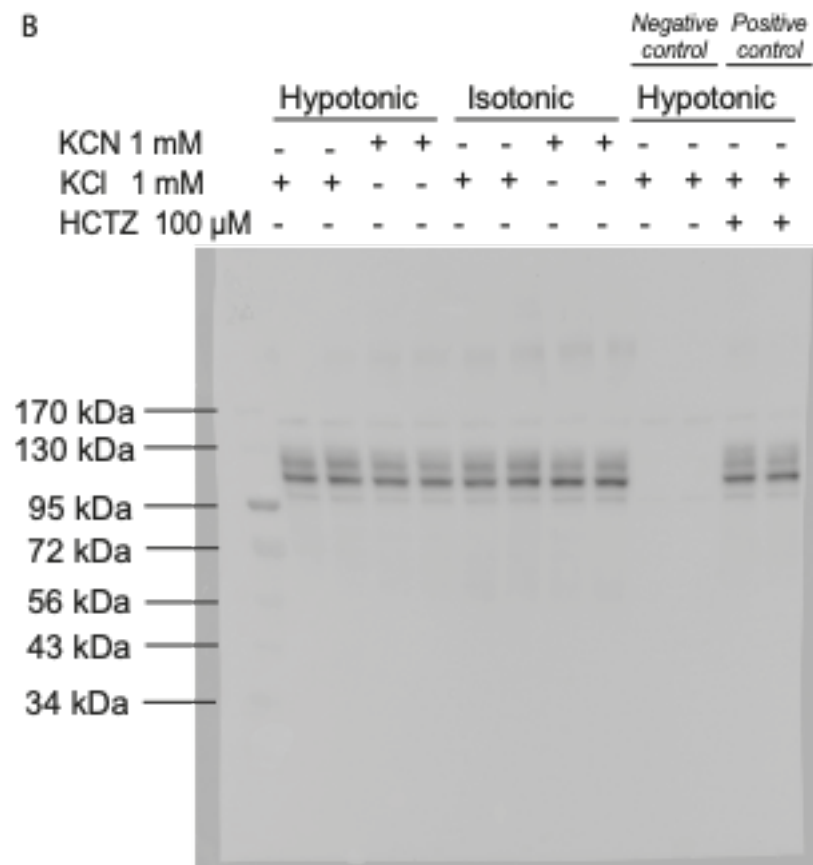
Control immunoblots of the $^{22}\text{Na}^+$ -uptake experiments in Figure 6. Numbers at the top indicate experiment number ($n = 4$). The legend indicates which HEK293 samples were transfected with NCC and which with mock. Size of NCC is 113 kDa, size of NCC dimers is 226 kDa. Primary antibody: rabbit anti-NCC (1:2000, Millipore, #AB3553); secondary antibody: peroxidase anti-rabbit-IgG (1:10 000, Sigma Aldrich, #A4914). The bands above at the top likely represent NCC dimers.

Supplementary Figure 4: Full immunoblot NCC phosphorylation experiments

A

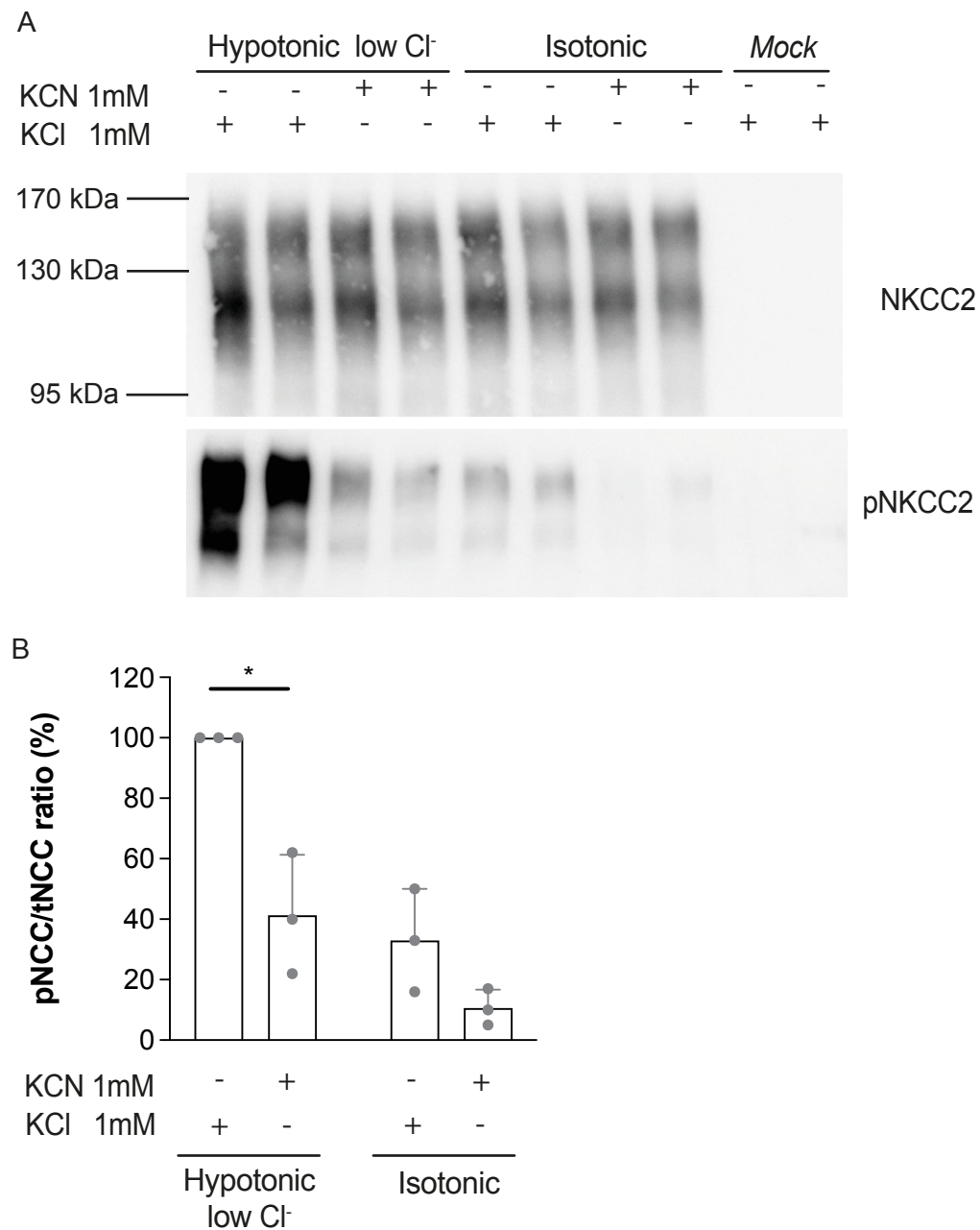


B



Full immunoblot of a representative experiment on which Figure 6 and its conclusions are based. Every experimental condition was cultured and blotted in duplicate; every experiment was executed three times. Size of NCC is 113 kDa. Negative control denotes the condition transfected with a mock expression vector instead of NCC expression vector. (A) Primary antibody: rabbit anti-pT58-NCC (NCC phosphorylated at human position p.Thr60, 1:2000, kind gift from Robert Fenton(8)); secondary antibody: peroxidase anti-rabbit-IgG (1:10 000, Sigma Aldrich, #A4914). Some non-specific bands are visible, as can be seen in the mock condition. Some bands might represent pNKCC1 (~160-200 kDa), which is a close homologue of NCC and has a phosphorylation site at a similar position. (B) Primary antibody: rabbit anti-NCC (1:2000, Millipore, #AB3553); secondary antibody: peroxidase anti-rabbit-IgG (1:10 000, Sigma Aldrich, #A4914). The bands at the top likely represent NCC dimers.

Supplementary Figure 5: NKCC2 phosphorylation with complex IV inhibition

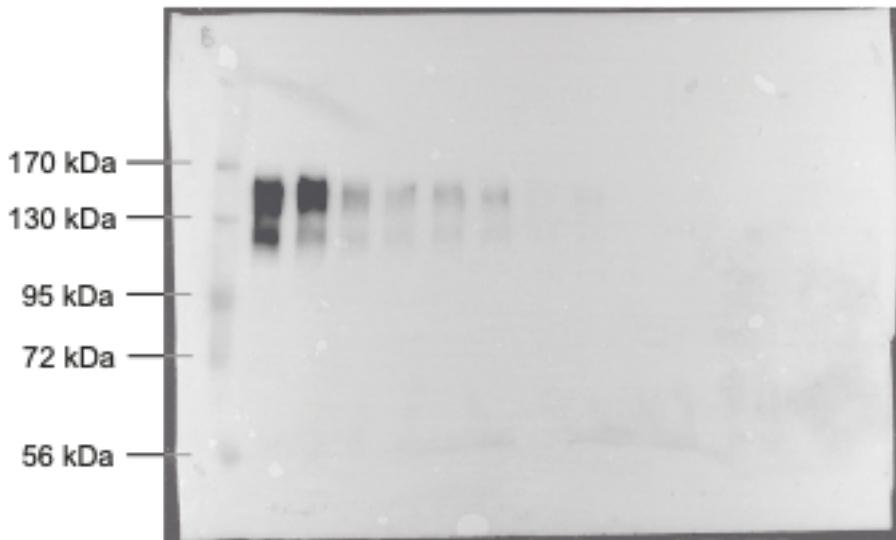


(A) Representative immunoblots showing NKCC2 and phosphorylated NKCC2 after a 30-minute incubation in hypotonic-low-chloride or isotonic buffer, with either KCN or KCl treatment. The mock condition has been incubated in hypotonic-low-chloride buffer as well. **(B)** Densitometry analysis of band intensity, pNCC/tNCC ratio (n = 3 of duplicates in each experiment). Significance was assessed with unpaired t-tests and corrected for multiple testing. KCN, potassium cyanide; KCl, potassium chloride; NKCC2, Na⁺-K⁺-Cl⁻-cotransporter; pNKCC2, NKCC2 isoform A phosphorylated at Ser91. *, p < 0.05.

Supplementary Figure 6: Full immunoblot NKCC2 phosphorylation experiments

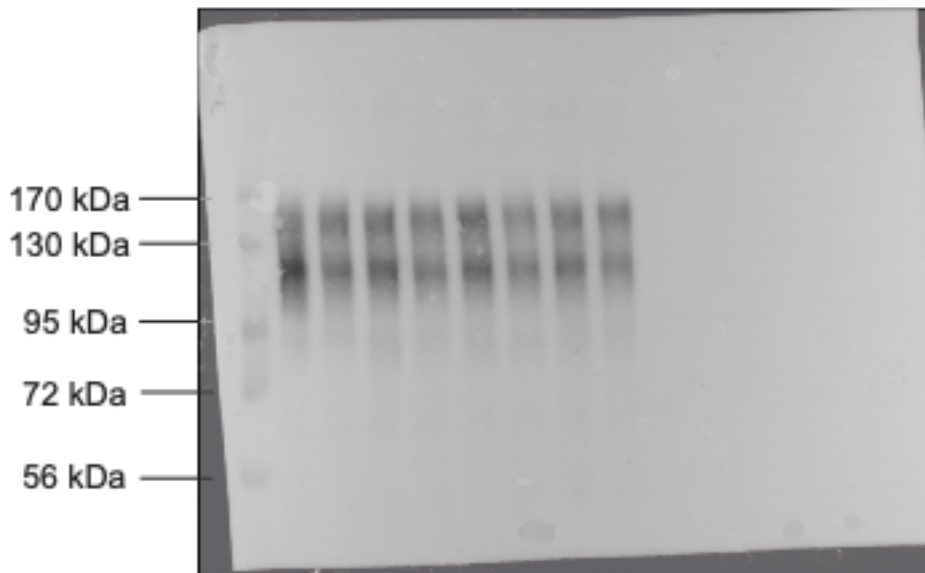
A

	Hypotonic				Isotonic				Negative control		
	Hypotonic		Isotonic		Isotonic		Hypotonic		Negative control		
KCN 1 mM	-	-	+	+	-	-	+	+	+	-	-
KCl 1 mM	+	+	-	-	+	+	-	-	+	+	+



B

	Hypotonic				Isotonic				Negative control		
	Hypotonic		Isotonic		Isotonic		Hypotonic		Negative control		
KCN 1 mM	-	-	+	+	-	-	+	+	+	-	-
KCl 1 mM	+	+	-	-	+	+	-	-	+	+	+



Full immunoblot of a representative experiment on which Supplementary Figure 5 is based. Every experimental condition was cultured and blotted in duplicate; every experiment was executed three times. Size of NKCC2 isoform A is 121 kDa. Negative control denotes the condition transfected with a mock expression vector instead of NKCC2 expression vector. (A) Primary antibody: sheep anti-pS91-NKCC2 (NKCC2 phosphorylated at human position p.Ser91,

1 µg/mL + 10 µg/mL non-phospho-peptide); secondary antibody: peroxidase anti-sheep-IgG (1:10 000, Jackson ImmunoResearch, #213-032-177). The upper band might represent residual glycosylated NKCC2, despite treatment with PNGase F. (B) Primary antibody: sheep anti-NKCC2 (1 µg/mL); secondary antibody: peroxidase anti-sheep-IgG (1:10 000, Jackson ImmunoResearch, #213-032-177). The upper band might represent residual glycosylated NKCC2, despite treatment with PNGase F.

References

1. Connor TM, Hoer S, Mallett A, Gale DP, Gomez-Duran A, Posse V, et al.: Mutations in mitochondrial DNA causing tubulointerstitial kidney disease. *PLoS genetics*, 13: e1006620, 2017
2. Bech AP, Wetzels JFM, Nijenhuis T: Reference values of renal tubular function tests are dependent on age and kidney function. *Physiol Rep*, 5, 2017 10.14814/phy2.13542
3. Colussi G, Bettinelli A, Tedeschi S, De Ferrari ME, Syrén ML, Borsa N, et al.: A Thiazide Test for the Diagnosis of Renal Tubular Hypokalemic Disorders. *Clinical Journal of the American Society of Nephrology*, 2: 454-460, 2007 10.2215/cjn.02950906
4. Bech AP, Wetzels JF, Bongers EMHF, Nijenhuis T: Thiazide Responsiveness Testing in Patients With Renal Magnesium Wasting and Correlation With Genetic Analysis: A Diagnostic Test Study. *American Journal of Kidney Diseases*, 68: 168-170, 2016 10.1053/j.ajkd.2015.12.023
5. Nozu K, Iijima K, Kanda K, Nakanishi K, Yoshikawa N, Satomura K, et al.: The Pharmacological Characteristics of Molecular-Based Inherited Salt-Losing Tubulopathies. *The Journal of Clinical Endocrinology & Metabolism*, 95: E511-E518, 2010 10.1210/jc.2010-0392
6. Rodenburg RJT: Biochemical diagnosis of mitochondrial disorders. *Journal of inherited metabolic disease*, 34: 283-292, 2011 10.1007/s10545-010-9081-y
7. Srere PA: [1] Citrate synthase: [EC 4.1.3.7. Citrate oxaloacetate-lyase (CoA-acetylating)]. In: *Methods in Enzymology*. Academic Press, 1969, pp 3-11
8. Pedersen NB, Hofmeister MV, Rosenbaek LL, Nielsen J, Fenton RA: Vasopressin induces phosphorylation of the thiazide-sensitive sodium chloride cotransporter in the distal convoluted tubule. *Kidney International*, 78: 160-169, 2010 10.1038/ki.2010.130
9. Wong LC, Chen T, Wang J, Tang S, Schmitt ES, Landsverk M, et al.: Interpretation of mitochondrial tRNA variants. *Genet Med*, 22: 917-926, 2020 10.1038/s41436-019-0746-0
10. Riedhammer KM, Braunisch MC, Günthner R, Wagner M, Hemmer C, Strom TM, et al.: Exome Sequencing and Identification of Phenocopies in Patients With Clinically Presumed Hereditary Nephropathies. *American Journal of Kidney Diseases*, 76: 460-470, 2020 <https://doi.org/10.1053/j.ajkd.2019.12.008>
11. Roshan M, Kabekkodu SP, Vijaya PH, Manjunath K, Graw J: Analysis of mitochondrial DNA variations in Indian patients with congenital cataract. 181-193, 2012
12. Lorenz R, Ahting U, Betzler C, Heimerling S, Borggrafe I, Lange-Sperandio B: Homoplasmy of the Mitochondrial DNA Mutation m.616T>C Leads to Mitochondrial Tubulointerstitial Kidney Disease and Encephalopathia. *Nephron*. 2019 pp 1-5 10.1159/000504412